Supplement of Geosci. Model Dev., 13, 537–564, 2020
https://doi.org/10.5194/gmd-13-537-2020-supplement

Geoscientific Model Development
Open Access
EGU

Supplement of

FORests and HYdrology under Climate Change in Switzerland v1.0: a spatially distributed model combining hydrology and forest dynamics

Matthias J. R. Speich et al.

Correspondence to: Matthias J. R. Speich (matthias.speich@wsl.ch, speichmatthias@gmail.com)

S1. Extended Methods

S1.1 Phenology module

S1.1.1 Module description

The phenological status variable $p_{d,sp}$, calculated daily in the leaf phenology module for each species and cell, is used to calculate daily LAI and FCC, as well as to define the start and end of the growing season. The range of $p_{d,sp}$ goes from zero (no leaves/winter dormancy) to one (fully developed foliage). Spring and autumn phenology are simulated with the models of Murray et al. (1989) and Delpierre et al. (2009), respectively.

The onset of leaf development in spring is modeled as a function of degree-day sum, counted from midwinter (January 15). The phenological status is zero until the degree-day sum reaches a threshold gdd_{min}. The value of this threshold varies as a function of accumulated chilling days (i.e. days with a mean temperature below a given threshold):

$$gdd_{min}(d) = a_{chill} + b_{chill} exp\left(-k_{chill} \times n_{chill}(d)\right), \quad \text{(S1)}$$

where $n_{chill}(d)$ is the number of chilling days since DOY 305 (November 1st), and a_{chill}, b_{chill} and k_{chill} are empirical parameters. Once gdd_{min} is reached, the phenological status is calculated as follows:

$$p_{d,sp}(d) = min\left(1, \frac{gdd(d) - gdd_{min}(d)}{r_{pg}}\right), \quad \text{(S2)}$$

where $gdd(d)$is the degree-day sum accumulated since January 15, and r_{pg} is an empirical parameter, controlling the rate at which leaf development occurs between bud burst and full foliage. Once the foliage is fully developed, the phenological status is set to one until the condition for the onset of leaf senescence is reached. The onset of leaf senescence is estimated using the model of Delpierre et al. (2009), based on day length and temperature. The state variable S_{sen} [arbitrary units] tracks the accumulation of conditions favoring the onset of leaf senescence:

$$S_{sen}(d) = S_{sen}(d-1) + R_{sen}(d), \quad \text{(S3)}$$

where $R_{sen}(d)$ is the daily time derivative of S_{sen}, calculated as follows:

$$R_{sen}(d) = \begin{cases} 0, p(d) \geq p_{dm} \; OR \; t(d) \geq t_{dm} \\ [t_{dm} - t(d)]^{x_{dm}} \times [p(d)/p_{dm}]^{y_{dm}}, otherwise' \end{cases} \quad \text{(S4)}$$

where $p(d)$ is day length [hours], $t(d)$ is mean temperature of the day d, and p_{dm}, t_{dm}, x_{dm} and y_{dm} are empirical parameters. The senescence state variable S_{sen} is only incremented if day length is less than p_{dm} and if temperature is below t_{dm}, whereas x_{dm} and y_{dm} express the relative sensitivity to temperature and photoperiod, respectively. The onset of senescence is defined as the day where S_{sen} reached a threshold value s_{dm} [arbitrary units]. Following the onset of senescence, for deciduous broadleaved trees, the phenological status is reduced linearly form one to zero over a period of 14 days. The summergreen conifer *Larix decidua* shows a smooth transition to the leafless state, with a slow decrease of foliage cover over several weeks to months (Migliavacca et al., 2008). Therefore, for this species, the S-shaped function proposed and parameterized by Scherstjanoi et al. (2014) is used:

$$p_{d,sp}(d) = \frac{1}{1 + 0.5 exp\left((13.5/d_{ls}) t_{ls} - 6.75\right)}, \quad \text{(S5)}$$

where t_{ls} is the day of senescence onset, estimated as described above, and d_{ls} is a pre-defined day on which the senescence process is assumed to be complete, defined here as DOY 335 (December 1st). The growing season is defined as the period where $p_{d,sp} \geq 0.5$ for the dominant species.

S1.1.2 Parameterization

The spring and autumn models were parameterized using visual observations at 20 stations of the Swiss meteorological office MeteoSwiss. Observations of leaf unfolding (LU) and leaf coloring (LC) were provided for ten of the species represented in FORHYCS. Table S1 gives an overview of the sites and species for which information was used. Observations of LU and LC for each site and species were retained if there are at least 15 records, in years for which complete time series of daily mean temperature are also available. Furthermore, sites were excluded if the elevation difference between the sites of temperature measurement and phenological observations was greater than 100 m.

Table S1: Overview of the phenological observations used at each station. lu: leaf unfolding, lc: leaf coloring. The elevation refers to the site where phenological observations were performed, which may differ from the location of the meteorological station. The stations were only retained if the elevation difference between both locations was less than 100 m.

	Acer pseudoplatanus	*Betula pendula*	*Castanea sativa*	*Corylus avellana*	*Fagus sylvatica*	*Larix decidua*	*Picea abies*	*Sorbus aucuparia*	*Tilia cordata*	*Tilia platyphyllos*
Adelboden (1350 m asl)	lu, lc	lu	-	lu	lu, lc	lu	lu	lu, lc	-	-
Altdorf (470 m asl)	lu, lc	lu	lu	lu	lu, lc	lu	lu	lu, lc	lc	lu, lc
Arosa (1900 m asl)	-	-	-	-	-	lu	-	-	-	-
Basel (315 m asl)	-	lu	-	lu	lu, lc	lu	lu	-	-	-
Chur (640 m asl)	lu, lc	lu	-	lu	lu, lc	lu	lu	lu, lc	lc	lc
Davos (1560 m asl)	-	lu	-	-	-	lu	lu	lu, lc	-	-
Disentis (1200 m asl)	lu	lu	-	lu	lu, lc	lu	lu	lu	-	lu, lc
Einsiedeln (910 m asl)	lu, lc	lu	-	lu	lu, lc	lu	lu	lu, lc	-	lu, lc
Elm (1000 m asl)	lu, lc	-	-	lu	lu, lc	lu	lu	lu, lc	lc	lu, lc
Hallau (430 m asl)	lu, lc	lu	lu	lu	lu, lc	lu	lu	lu, lc	lc	lu, lc
La Brévine (1050 m asl)	lu	lu	-	lu	lu, lc	lu	lu	lu, lc	-	lu
Locarno (370 m asl)	-	-	-	lu	-	-	-	lu, lc	-	lu, lc
Nyon-Changins (435 m asl)	lu	lu	lu	lu	lu, lc	lu	lu	-	-	-
San Bernardino (1625 m asl)	-	-	-	-	-	lu	-	-	-	-
Schiers (700 m asl)	-	-	-	lu	lu, lc	lu	lu	-	-	-
Scuol (1240 m asl)	lu, lc	lu	-	lu	lu, lc	lu	lu	lu, lc	lc	lc
Sta. Maria (1390 m asl)	-	lu	-	lu	-	lu	-	lu, lc	-	-
Visp (650 m asl)	-	-	-	-	-	lu	-	-	-	-

Zurich (555 m asl)	-	lu	-	lu	lu, lc	lu	lu	lu, lc	lc	lu, lc

The spring and autumn models were calibrated separately, both using the Latin hypercube sampling approach, which is a stratified Monte-Carlo sampling. In both cases, 500 parameter sets were generated, and the calculated dates of leaf unfolding or leaf coloration were compared with the observations. The simulated date of leaf unfolding was defined as the first day of the year where $p_{d,sp}$ exceeds 0.5, and the simulated date of leaf coloring as the first day in autumn where $p_{d,sp}$ is no longer one. As goodness-of-fit measures, the mean absolute error (MAE) [days] and the Nash-Sutcliffe efficiency (NSE) (Nash and Sutcliffe, 1970) were calculated:

$$MAE = \frac{\sum_{i=1}^{n}|sim_i - obs_i|}{n}, \quad \text{(S6)}$$

$$NSE = 1 - \frac{\sum_{i=1}^{n}(sim_i - obs_i)^2}{\sum_{i=1}^{n}(obs_i - \overline{obs})^2}, \quad \text{(S7)}$$

where n is the number of years for which both observed and simulated leaf unfolding or leaf coloring values were available, sim_i and obs_i the simulated and observed dates of LU or LC for the year i, expressed as DOY, and $\overline{obs}$ the mean of the n observations. The NSE takes values between $-\infty$ and 1, where 1 indicates a perfect fit, and 0 indicates that the model is as good a predictor as the mean of the observations.

Although the parameters of the spring and autumn models all have a certain meaning, they are not physically measurable quantities. Therefore, their parameterization involves a certain degree of arbitrariness. In both models, there are strong interactions between some parameters, and the value of one parameter has no particular meaning without knowing the value of the other. It is therefore possible to reduce the number of calibration parameters by fixing the value of one parameter. For the spring model, the value of k_{chill} was fixed to 0.05, whereas the values of the other parameters were varied. For the autumn model, the value of s_{dm} was fixed to a value of 100. Table S2 shows the remaining calibration parameters and their range.

Table S2: Calibration parameters for the spring and autumn senescence models. Ranges were defined based on previous applications of the models (e.g. Delpierre et al. (2009)).

Parameter	**Unit**	**Range**
a_{chill}	degree days (K d)	0 – 200
b_{chill}	degree days (K d)	100 – 1000
r_{pg}	degree days (K d)	100 – 400
p_{dm}	hours	10 – 15.5
t_{dm}	°C	7 – 30
x_{dm}	-	0 – 2
y_{dm}	-	0 – 2

For each phenological phase and species, the maximum MAE over all stations was determined. The retained parameter set is the one with the lowest maximum MAE. Table S3 shows the retained parameter sets for the spring model, and Table S4 for the autumn model.

Table S3: Selected parameter sets for the spring phenology model. The number n indicates the number of stations for which there were enough observations available.

	a_{chill}	b_{chill}	r_{pg}	Best MAE [days]	Worst MAE [days]	Best ME [-]	Worst ME [-]
Acer pseudoplatanus (n=10)	85.64	927	103	3.72	12.25	0.25	-3.95
Betula pendula (n=13)	0.19	648	185	4.16	14.2	0.63	-5.15
Corylus avellana (n=15)	6.13	798	193	5.53	13.78	0.37	-2.26
Castanea sativa (n=3)	157	960	144	3	5.75	0.25	-0.44
Fagus sylvatica (n=13)	8	730	249	5.24	13.29	0.28	-4.03
Larix decidua (n=18)	3.81	967	141	4.88	13.82	0.47	-3.85
Picea abies (n=14)	2.19	983	331	5.36	14.45	0.52	-4.2
Sorbus aucuparia (n=13)	6.85	745	165	3.48	12.47	0.53	-2.87
Tilia platyphyllos (n=10)	48	993	221	3.89	14.31	0.37	-3.31

Table S4: Selected parameter sets for the autumn phenology model. The number n indicates the number of stations for which there were enough observations available. (*) In the case of Larix decidua*, the parameters were visually fit to match weekly observations of foliage status, as described in the text.*

	p_{dm}	t_{dm}	x_{dm}	y_{dm}	Best MAE [days]	Worst MAE [days]	Best ME [-]	Worst ME [-]
Acer pseudoplatanus (n=7)	15.16	23.1	0.361	1.805	5.67	17.6	-0.14	-5.98
Fagus sylvatica (n=13)	12.1	17.57	1.824	1.65	11.88	25.48	-0.05	-3.99
Larix decidua	13	22	0.75	1	-	-	-	-

(*)								
Sorbus aucuparia (n=9)	14.73	23.31	0.291	0.469	8.59	12.95	-0.08	-2.04
Tilia cordata (n=6)	12.93	29.61	0.446	0.411	8.94	10.19	0.06	-0.85
Tilia platyphyllos (n=9)	13.71	18.36	0.476	0.489	5.95	17	0.02	-3.07

The spring models are able to predict the date of bud burst with an error ranging between three days and two weeks. For the autumn models, the error is somewhat larger, up to 25 days for *Fagus sylvatica*. At individual stations, the Delpierre model achieved better performance, but the optimal parameter sets were not consistent between the stations. This suggests that it is difficult to model the onset of leaf senescence across different climatic zones, particularly for some species. Nevertheless, this model was adopted in FORHYCS, as it is more robust than other methods tested (including temperature threshold methods or specifying a fixed cumulative sum of $p_{d,sp}$). The NSE scores indicate that the models were generally not able to outperform the mean of observations for the timing of autumn phenology. This is consistent with other studies (e.g. Olsson and Jönsson, 2015). For the species for which no observations are available, the parameter sets of the observed species are assigned, as shown in Table S5.

Table S5: Assignment of species-specific parameter sets to species for which no observations are available. A dash indicates that observations were available for either spring or autumn, but not for the other season.

Species	**Spring parameter set**	**Autumn parameter set**
Evergreen conifers	*Picea abies*	*Larix decidua*
Acer spp., Quercus spp.	*Acer pseudoplatanus*	*Acer pseudoplatanus*
Alnus spp., Salix alba, Sorbus aria	*Sorbus aucuparia*	*Sorbus aucuparia*
Betula pendula	-	*Sorbus aucuparia*
Carpinus betulus, Fraxinus excelsior, Populus spp., Ulmus scabra	*Fagus sylvatica*	*Fagus sylvatica*
Castanea sativa	-	*Fagus sylvatica*
Corylus avellana	-	*Sorbus aucuparia*
Tilia cordata	*Tilia platyphyllos*	-

While the beginning of the growing season for evergreen conifers can be assumed to correspond to the date of leaf unfolding, there are no easily observable variables that indicate the end of the growing season. The parameterization of autumn phenology for conifers is based on weekly visual observations of the foliage status of the deciduous conifer *Larix decidua* in the valley of Lötschental in the Central Swiss Alps, ranging between 1300 and 2200 m asl (Moser et al., 2010). Whereas for evergreen conifers, LAI is kept

constant throughout the year, the calculation of $p_{d,sp}$ is used to estimate the start and end of the growing season. The development of s_{phen} after the onset of leaf senescence is modeled using the senescence function for larch (Eq. S5). As for deciduous species, the growing season is defined as the period where $p_{d,sp}$ is greater than 0.5.

S1.2 Effect of low temperature and nitrogen in TreeMig

The three bioclimatic indices that impact growth and mortality in TreeMig represent water availability and temperature, and nitrogen availability. The first index, representing drought, is discussed in the main text (Eqs. 5 and 6). Temperature is represented by annual degree-day sums. The temperature-dependent vitality function (analogous to Eq. 6) is defined as:

$$f_{DD} = MAX\left(0{,}1 - exp\left(\frac{1.386(k_{DDmin} - DDEGS)}{k_{DD75}}\right)\right) \quad \text{(S8)}$$

where DDEGS is the annual degree-day sum and k_{DDmin} and k_{DD75} are species-specific parameters, indicating the minimum DDEGS value required by a species, and the additional degree-day sum necessary so that $f_{DD}(k_{DDmin}+k_{DD75}) = 0.75$. This function saturates as temperature increases, so that forest growth may be limited by low, but not by high temperature.

The effect of nitrogen availability is reflected in the index f_N:

$$f_N = MAX\left(0{,}1 - exp(k_{N1} \times N_{av} - k_{N2})\right) \quad \text{(S)}$$

where k_{N1} and k_{N2} are species group-specific empirical parameters, and N_{av} is nitrogen availability. In this study, N_{av} is kept spatially and temporally constant. Therefore, there is no simulation of nitrogen-related processes in this study.

These three environment-dependent functions are combined into a single vitality reduction function using the geometric mean:

$$f_{env} = \sqrt[3]{f_{DS} \times f_{DD} \times f_N} \quad \text{(S)}$$

where f_{DS} is the drought-dependent stress function (Eq. 6 in the main text). The environment-dependent vitality reduction function influences tree growth and mortality, as described by Lischke et al. (2006).

S1.3 Allometric equations for leaf area calculations

Leaf area calculation in FORHYCS is based on allometric functions parameterized by Bugmann (1994) (see Section 2.1.2 in the main text). The basis for this parameterization was a dataset collected by Burger (1929 - 1953), consisting of measurements of tree height, diameter and leaf area on 583 trees of five species or species groups. Tree species not represented in the dataset are assigned to one of the represented species, still following Bugmann (1994). The number of trees for each species, and specific parameters are given in the appendix of Bugmann (1994). Since this document is not widely available, we repeat this information here. Specific leaf area (SLA) is set to 6 m^2kg^{-1} for coniferous species and 12 m^2kg^{-1} for broadleaved species. The empirical parameters $a_{1,sp}$ and $a_{2,sp}$ are reported in Table S6, along with the sample size used by Bugmann (1994).

Table S6: values for the empirical parameters used in the allometric function relating diameter at breast height to leaf area (Eq. 1 in the main text).

Species	$a_{1,sp}$	$a_{2,sp}$	n
Abies alba, Picea abies, Pinus cembra, P. montana	0.23	1.56	130
Pinus sylvestris	0.17	1.4	210
Fagus sylvatica, Quercus spp.	0.06	1.7	144
Larix decidua	0.1	1.43	99
Betula alba, Salix alba	0.08	1.43	(no data)

S1.4 Species-specific drought tolerance parameters

Table S7: Values for the species-specific drought tolerance parameter kDT used in this study (last column). The parameter values were obtained by mapping the drought tolerance scores of Niinemets and Valladares (2006) (second column) on the range of values used by Lischke and Zierl (2002). Some of the parameter values were adjusted manually to improve modeled species composition. The parameters of Lischke and Zierl (2002) and of this study indicate the drought index DI at which the drought stress function (Eq. 6) becomes zero. The scores of Niinemets and Valladares (2006) take values between 1 (low tolerance) and 5 (high tolerance) and were obtained based on climatic characteristics at sites where each species was observed. Species marked with an asterisk were excluded from the simulations presented in this paper.

Species	Drought tolerance parameter in Lischke and Zierl (2002)	Drought tolerance according to Niinemets and Valladares (2006)	Drought tolerance parameter used in this study
Abies alba	0.37	1.81	0.28
Larix decidua	0.45	2.31	0.42
Picea abies	0.41	1.75	0.32
Pinus cembra	0.43	3.01	0.45
Pinus montana	0.4	4.23	0.49
Pinus sylvestris	0.55	4.43	0.45
Taxus baccata	0.39	3.01	0.38
Acer campestre	0.46	2.93	0.37
Acer platanoides	0.42	2.73	0.36
Acer pseudoplatanus	0.34	2.75	0.32
Alnus glutinosa	0.37	2.22	0.31
Alnus incana	0.34	1.89	0.28
Alnus viridis	0.37	2.48	0.33
Betula pendula	0.35	1.85	0.28
Carpinus betulus	0.46	2.66	0.35
Castanea sativa*	0.3	3.46	0.42
Corylus avellana	0.46	3.04	0.38
Fagus sylvatica*	0.37	2.4	0.33
Fraxinus excelsior	0.39	2.5	0.34
Populus nigra	0.3	2.2	0.31
Populus tremula	0.41	2.85	0.37
Quercus petraea	0.44	3.02	0.38
Quercus pubescens	0.4	4.1	0.48
Quercus robur	0.44	2.95	0.38
Salix alba	0.39	2	0.29
Sorbus aria	0.38	3.55	0.43
Sorbus aucuparia	0.27	2.11	0.3

Tilia cordata	0.4	2.75	0.36
Tilia platyphyllos	0.4	2.52	0.34
Ulmus scabra	0.35	2.41	0.33

S1.5 Local water balance module

S1.5.1 Summary of module

Canopy transpiration and soil evaporation are simulated with the hybrid dual-source model of Guan and Wilson (2009). The term "hybrid" refers to two concepts used to partition latent heat flux between canopy and soil, the layer approach (where the available energy is split between canopy and soil based on LAI) and the patch approach (where the energy and vapor fluxes are calculated independently for vegetated and non-vegetated patches, based on fractional cover). The scheme of Guan and Wilson combines these two approaches, by partitioning total available energy (R_n, the sum of net shortwave and longwave radiation [W m^{-2}]) into canopy and soil fractions (A_c and A_s, respectively) based on LAI, and by calculating latent heat flux for each compartment based on fractional cover. This way, the model is applicable to both sparse and dense canopies (Guan and Wilson, 2009). This submodel was tested in different ecosystems (Lu et al., 2014) and outperformed similar formulations, i.e. the widely used Penman-Monteith (Monteith, 1965) and Shuttleworth-Wallace (Shuttleworth and Wallace, 1985) approaches.

Details on the calculation of shortwave and longwave radiation are given in the appendix. The partitioning of R_n between canopy and soil is done with Beer's law:

$$A_c = R_n\left(1 - exp(-k_c LAI)\right), \quad \text{(S9)}$$

$$A_s = \left[R_n\left(exp(-k_c LAI)\right)\right]\times(1 - f_{SF}), \quad \text{(S10)}$$

where k_c is the canopy light extinction coefficient, and f_{SF} the fraction of energy reaching the soil that is lost as soil heat flux. First, evaporation of intercepted (E_{Int}) water is estimated, assuming no surface resistance. The estimation of E_{Int} is explained in the Appendix. The next step is the calculation of canopy transpiration:

$$E_{T,act} = \frac{\Delta A_t + FVC\frac{\rho_a c_p}{r_a}(VPD)}{\left[\Delta+\gamma\left(\frac{r_s^c}{r_a}\right)\right]\rho_w \lambda}\times(1 - F_{wet}), \quad \text{(S11)}$$

where Δ is the first derivative of the relationship between saturated vapor pressure and temperature [hPa K^{-1}], A_t the available energy for transpiration (after the energy used for interception evaporation has been subtracted from A_c), ρ_a the density of air [kg m^{-3}], c_p the heat capacity of air [J kg^{-1} K^{-1}], r_a^a and r_a^c are the above-canopy and within-canopy aerodynamic resistances, respectively [s m^{-1}], VPD the difference of saturated and actual atmospheric water vapor pressure [hPa], γ the psychrometric "constant" [hPa K^{-1}], ρ_w the density of water [kg m^{-3}], λ the latent heat of vaporization of water [J kg^{-1}], and F_{wet} is the fraction of foliage area covered by water. Details on the estimation of aerodynamic resistances and foliage wetness are given in the supplementary material of Speich et al. (2018).

The term r_s^c is the surface resistance of the forest canopy [s m^{-1}]. It is estimated using a Jarvis-type formulation (Jarvis, 1976), where a minimum stomatal resistance RSMIN, is scaled by LAI and multiplied by functions of environmental conditions:

$$r_s^c = \frac{RSMIN}{LAI/FVC} f_1(R_g) f_2(T_a) f_3(VPD) f_4(SSM) f_5(CCA), \quad \text{(S12)}$$

where R_g is global radiation [W m^{-2}], T_a is air temperature [°C] and CCA the atmospheric CO_2 concentration. The radiation response function is implemented following Stewart (1988):

$$f_1 = \frac{1000}{1000+j_R} \times \frac{R_g+j_R}{R_g}, \quad \text{(S13)}$$

where j_R is an empirical parameter set to 100 [W m^{-2}]. The temperature response function is also taken from Stewart (1988):

$$f_2 = \frac{(T_a-TMIN)(TMAX-T_a)^a}{(TOPT-TMIN)(TMAX-TOPT)^a}, \quad \text{(S14)}$$

where

$$a = \frac{TMAX-TOPT}{TOPT-TMIN}, \quad \text{(S15)}$$

and TMIN, TOPT and TMAX are the minimum, optimal and maximum temperatures for photosynthesis, set here to 0, 18 and 40 °C. For the effect of VPD, a negative exponential effect on stomatal conductance (the inverse of resistance) is assumed (Braun et al., 2010):

$$f_3 = 1/\exp(-j_{VPD} \times VPD). \quad \text{(S16)}$$

Based on a preliminary analysis of sap flow records of conifers in plots close to the test area (Richard Peters et al., WSL, unpublished data), j_{VPD} was set to 0.08 hPa^{-1}. For soil moisture, a linear effect on conductance is assumed below a certain threshold of relative extractable water, j_{SM}, set to 0.4 (Granier et al., 1999):

$$f_4 = \begin{cases} 1 \; if \; \frac{SSM_t}{SFC} \geq j_{SM} \\ \frac{j_{SM} \times SFC}{SSM_t} \; otherwise \end{cases}. \quad \text{(S17)}$$

The newly implemented drought index (see Section 2.1.3) requires an estimate of potential transpiration ($E_{T,pot}$), the hypothetical transpiration rate obtained by ignoring the effects of dry air and dry soil on canopy resistance (Zierl, 2001). Potential transpiration is calculated using Eq. TODO, with the surface resistance defined as:

$$r^c_{s,pot} = \frac{RSMIN}{LAI/FVC} f_1(R_g) f_2(T_a) f_5(CCA). \quad \text{(S18)}$$

For soil evaporation, instead of explicitly parameterizing a surface resistance, an exponential reduction of potential evaporation with increasing number of rain-free days is implemented, following Morillas et al. (2013).

S1.5.2 Parameterization of minimum stomatal resistance

In coupled FORHYCS, minimum stomatal resistance is parameterized as a function of simulated species-size distribution. Species are divided into three classes, with minimum stomatal resistance values corresponding to 125, 180 and 333 s m^{-1}, respectively. In addition, the model assumes a linear decrease of stomatal conductance (the inverse of resistance) of 0.02 s m^{-1} per additional meter tree height (based on results by Ford et al., 2011). A canopy-level value of minimum stomatal resistance is calculated by averaging the obtained resistance over all species-size classes, weighted by their share of stand leaf area.

S1.6 Comparison of soil water storage datasets

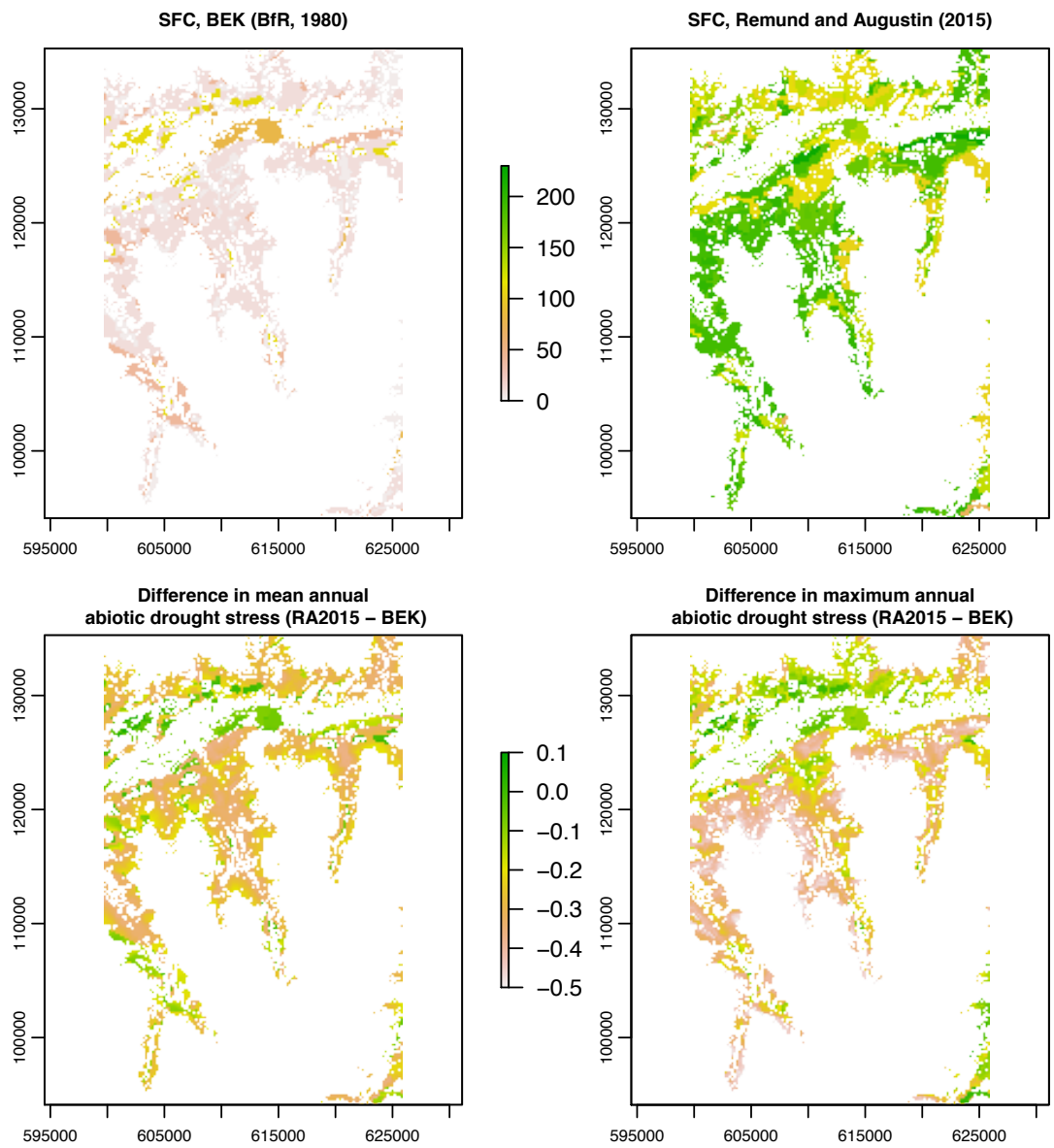

Figure S1: Comparison of the two datasets for soil moisture storage capacity used in this study. The top panels represent the soil moisture storage capacity [mm] for the BEK (left) and RA2015 datasets (right).The bottom panels show the difference in mean (left) and maximum (right) abiotic drought stress calculated over the period 1971-2015. Values are positive if the drought index was greater (i.e. higher stress) with the RA2015 dataset, and negative if the index was greater with the BEK dataset.

S1.7 PREVAH parameterization

S1.7.1 Land cover-specific parameters

As noted in Sect. 2.1.8, non-forested but vegetated land cover classes were assigned a rooting depth parameter. As the soil water storage capacity of Remund and Augustin (2015) generally assumes a depth of 1 m, available water storage capacity in a cell is obtained by multiplying the cell-specific storage capacity with the land cover-specific rooting depth value. Table S6 gives the prescribed rooting depth for the various land cover types. These values are based on the ratios between various land cover types and forests in Hough and Jones (1997). Non-vegetated land cover types use the same soil parameterization as

in earlier versions of PREVAH (Gurtz et al., 1997). In addition, in simulations where the dynamic rooting depth module is disabled, a constant rooting depth of 1 m is assumed for forests.

Table S8: Prescribed rooting depth for non-forested, vegetated land cover classes

Land cover categories	**Rooting depth [m]**
Agricultural land cover classes	0.44
Orchards	0.53
Meadows; alpine vegetation	0.22

S1.7.2 Tuneable and spatially distributed parameters

PREVAH has a number of parameters not related to vegetation. These consist of 14 spatially distributed parameters. The parameter values for this study were taken from a previous application of PREVAH, where the long-term water balance was simulated for all of Switzerland (Zappa and Bernhard, 2012), with a manual tuning of 5 parameters to improve the optical fit of simulated daily streamflow (Fig. 5 in the main text). Due to the proof-of-concept nature of this study, a full calibration was not undertaken. However, we argue that some tuning of the parameters is justified, as the dataset for soil depth and storage capacity differs greatly from the one used in previous applications of PREVAH (see Section 2.2.2 in the main text).

S1.8 Climate characteristics of the GCM-RCM chains

The following figures show some climatic characteristics of the three GCM-RCM chains used to drive the model in this case study. The characteristics of precipitation (annual sum, event frequency and mean event depth) are shown on Figs S2-S4 for the five subcatchments for which streamflow is evaluated (all figures for precipitation are shown as 30-year rolling averages). For temperature, mean annual and mean growing season (May-October) temperatures are shown on Fig. S5 for two arbitrarily selected cells (one at the bottom of the main valley at 667 m asl, and one near the treeline at 2160 m asl.)

S1.9 Reconstruction of observed streamflow time series

The water of the Gougra and Navizence streams is used for hydropower generation, which impacts the timing of observed streamflow. In particular, a reservoir lake stores the inflow of subcatchment 5 (Moiry/Lona). In addition, water from the exit of subcatchment 4 (Mottec) and from a neighboring catchment can be pumped into the reservoir lake, and water from the reservoir can be diverted to be turbinated at the exit of subcatchment 4. An overview of the location of the reservoir lake and diversions is given by Alpiq (2014). As a result, observed streamflow does not correspond to the streamflow that would occur naturally in the subcatchments 3 (Vissoie) and 5 (Moiry/Lona). The raw streamflow data, provided by the power plant operator, include (1) water intake at the power plants, (2) the amount of water pumped from inside and from outside the catchment into the reservoir lake, (3) variations in the storage content of the reservoir, and (4) the amount of water diverted from the reservoir to be turbinated at the exit of subcatchment 4. For subcatchment 3, the daily streamflow used in this study only consider the water originating from this subcatchment, i.e. water coming from subcatchments 4 and 5 and from

outside the catchment is not counted. For subcatchment 5, daily streamflow was reconstructed by adding the daily change in reservoir volume and the amount of water diverted to be turbinated, and subtracting the amount of water pumped into the reservoir. For subcatchments 2 and 4, the amount of water measured at the turbine intake was assumed to correspond to daily streamflow. These values therefore do not account for residual flows and variations in the tailwater reservoirs, which are assumed to be small at a daily timescale.

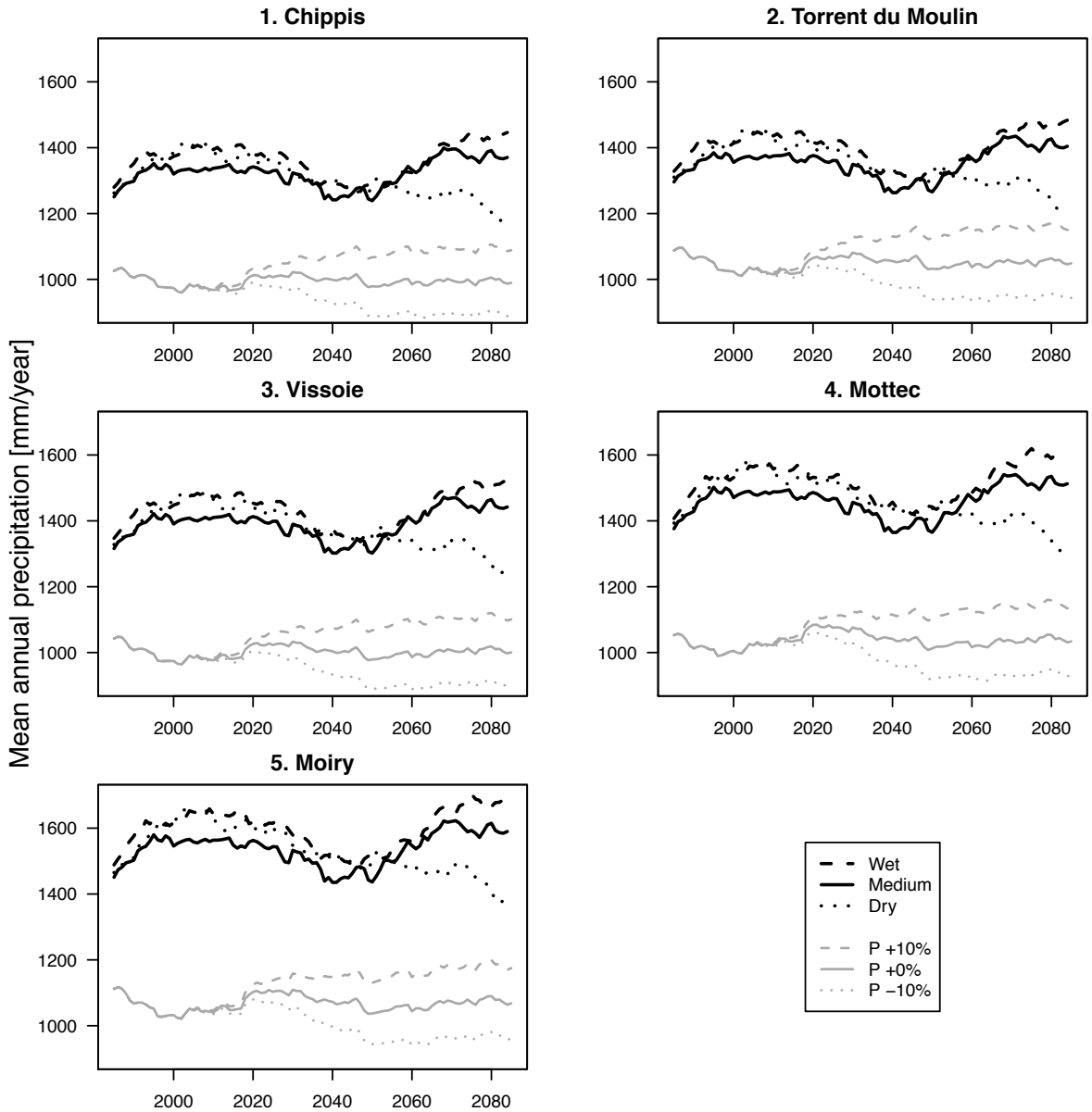

Figure S2: Mean annual precipitation sums for the delta change runs (grey lines) and runs with GCM-RCM chains (black lines). All values are 30-year rolling means.

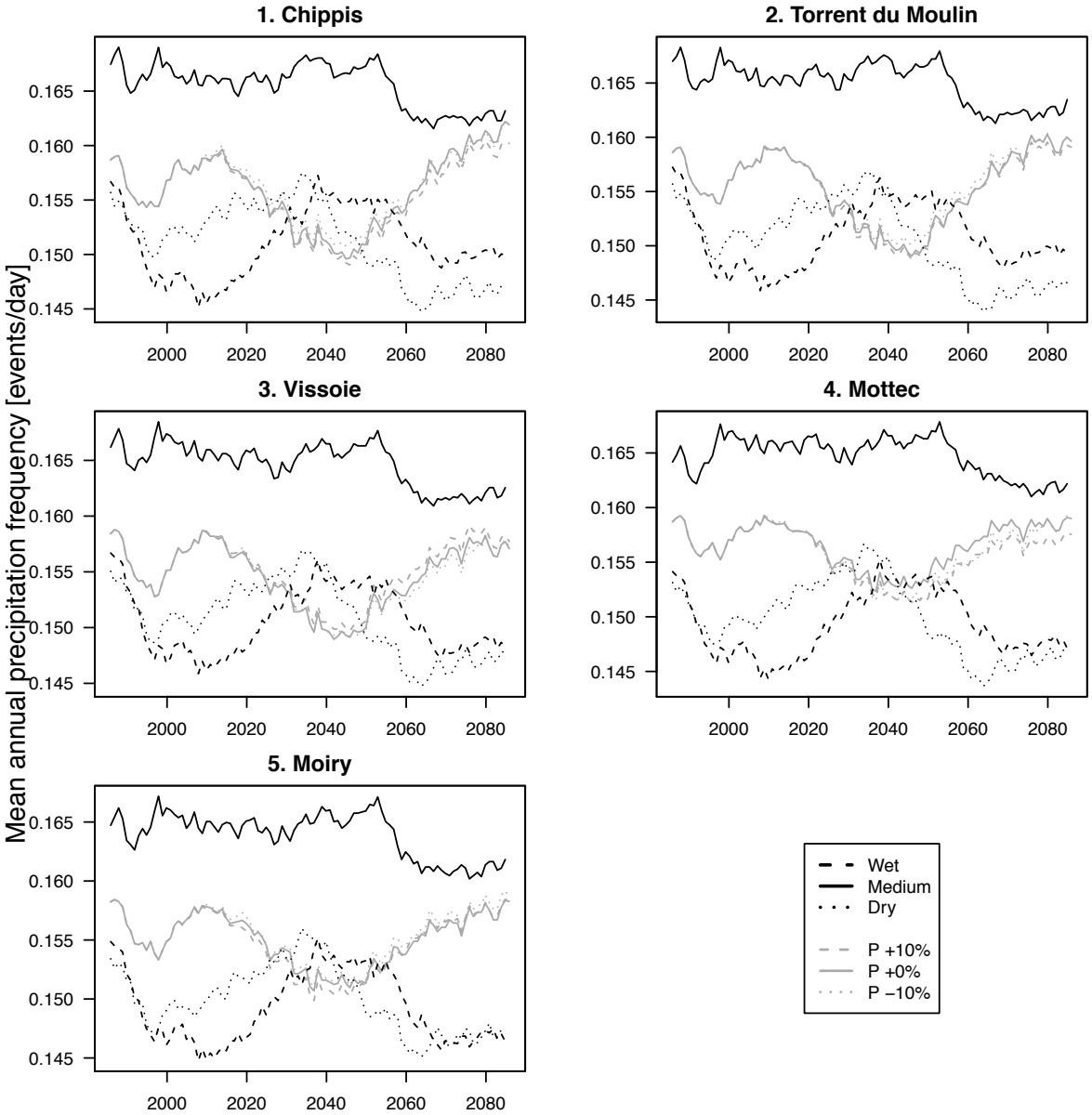

Figure S3: Mean annual precipitation frequency for the delta change runs (grey lines) and runs with GCM-RCM chains (black lines). All values are 30-year rolling means.

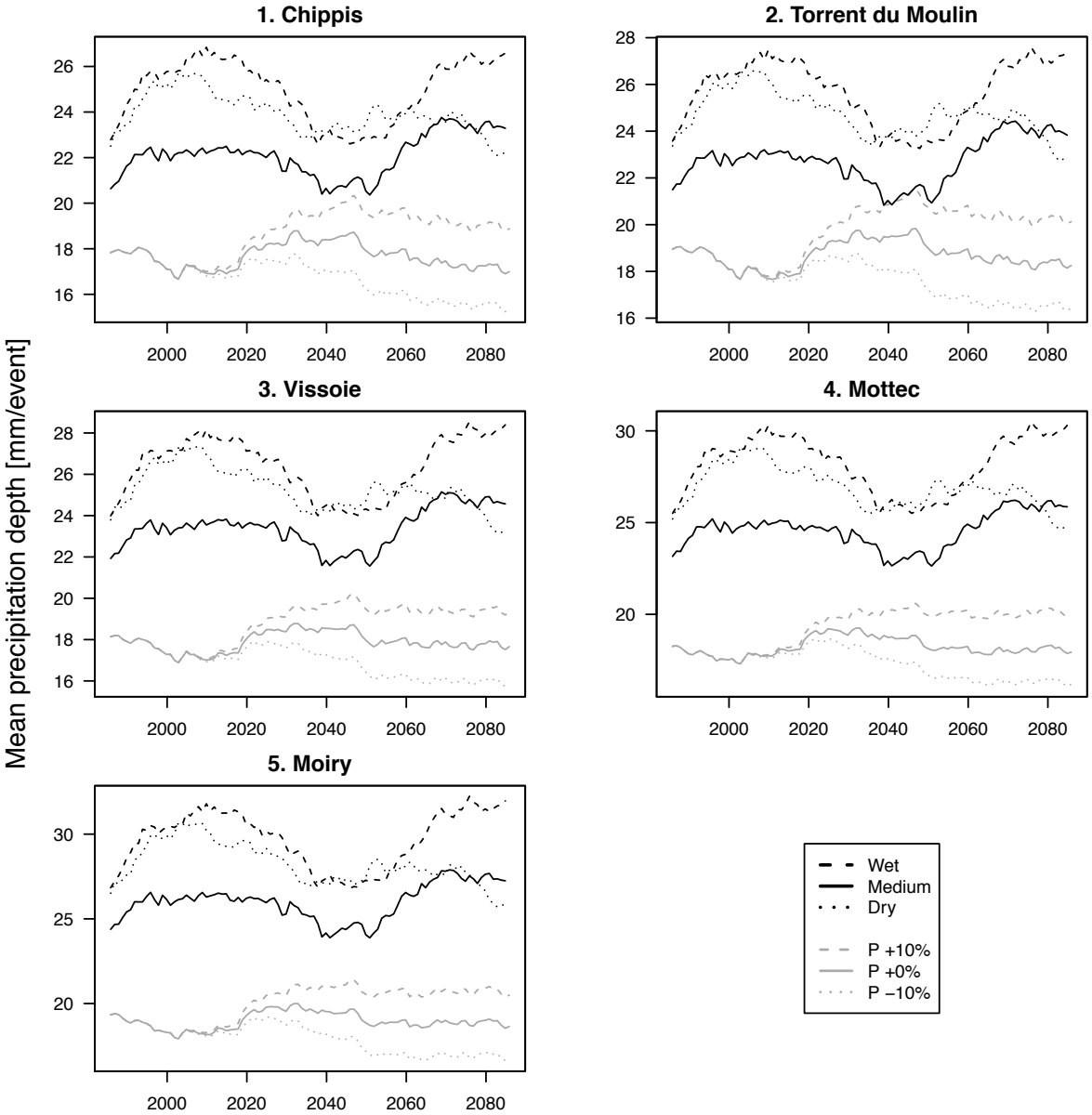

Figure S4: Mean precipitation intensity for the delta change runs (grey lines) and runs with GCM-RCM chains (black lines). All values are 30-year rolling means.

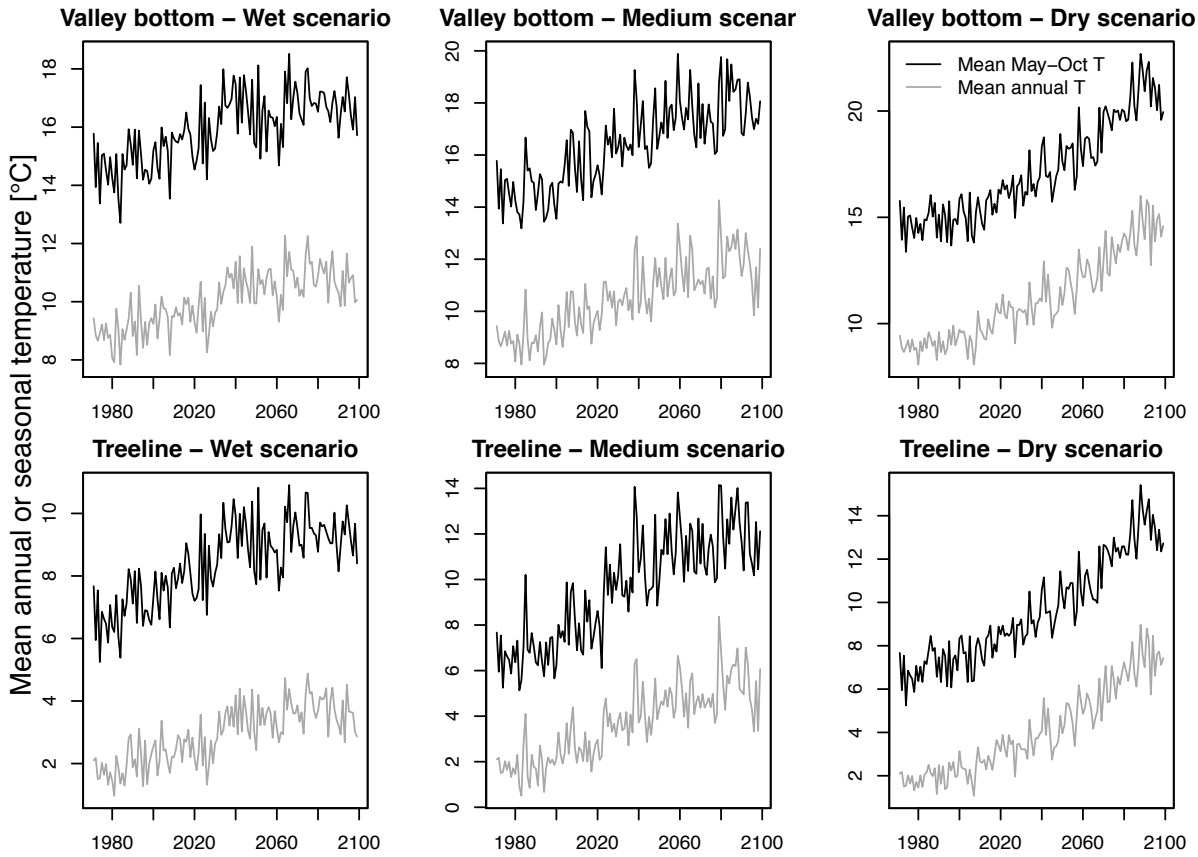

Figure S5: Mean seasonal (May-October) and annual temperatures for two arbitrarily selected cells of the study domain (Valley bottom: 667 m asl; Treeline: 2160 m asl), for the three GCM-RCM chains used in this study.

S2. Extended results

S2.1 Streamflow plausibilization for subcatchments 2, 4 and 5

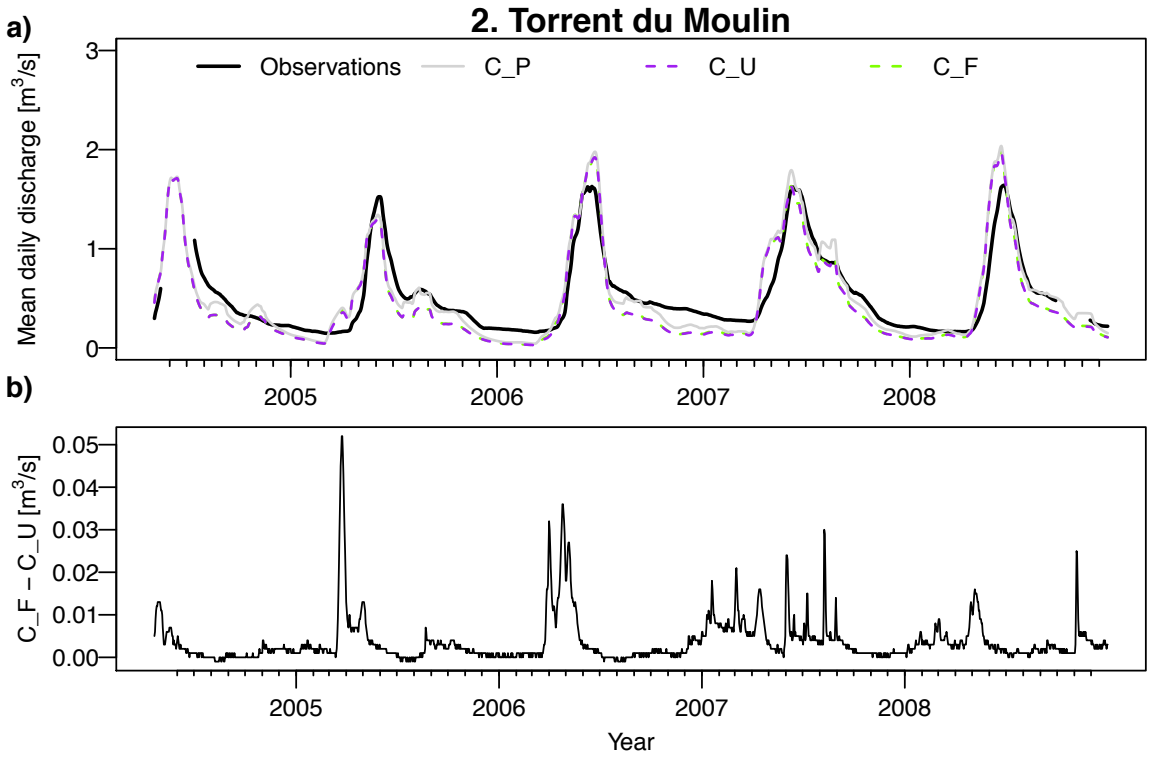

Figure S6: (a) Observed vs. simulated daily streamflow for subcatchment 2 (Torrent du Moulin) for the period 2004-2008. For clarity, the plot shows rolling averages with a 30-day window. The plot shows results for two FORHYCS runs, uncoupled (C_U) and fully coupled (C_F). For reference, the results obtained with standard PREVAH (C_P) are also shown. (b) Difference in simulated daily streamflow between the coupled and uncoupled versions of FORHYCS. Unlike in a), values are not shown as rolling averages. Streamflow simulated with coupled FORHYCS is usually higher than for the uncoupled version, and the greatest differences occur in winter and spring.

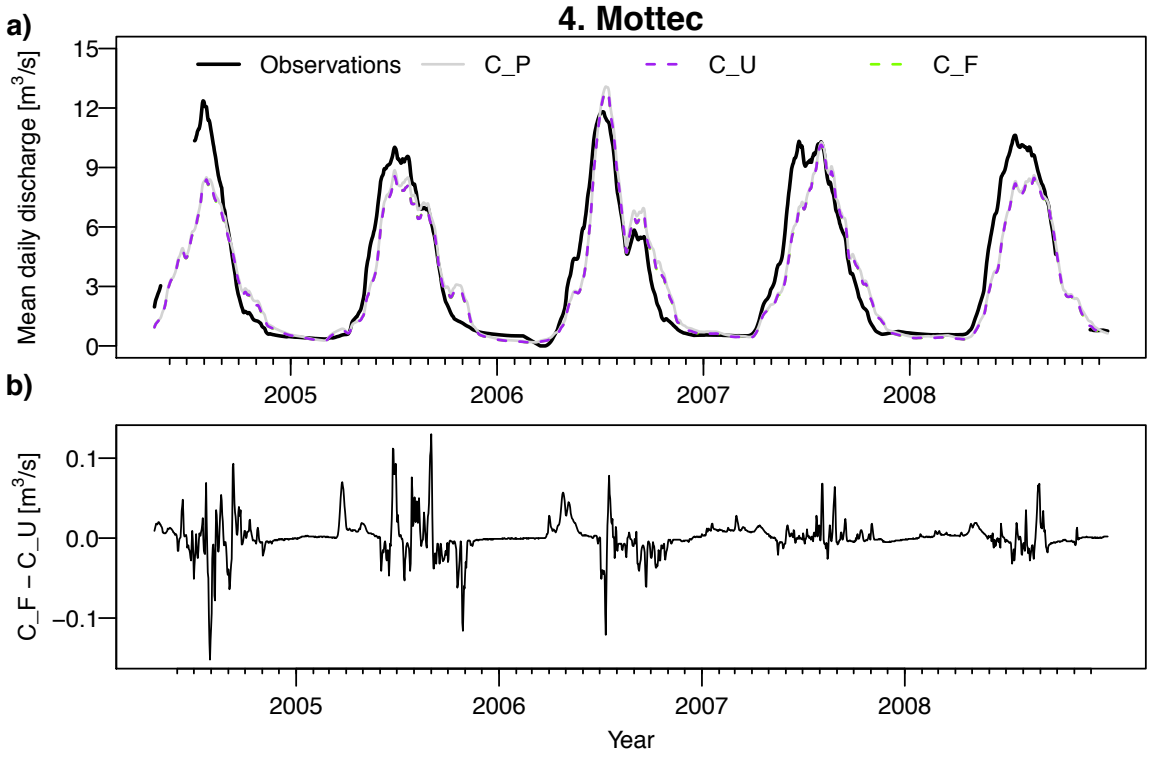

Figure S7: (a) Observed vs. simulated daily streamflow for subcatchment 4 (Mottec) for the period 2004-2008. For clarity, the plot shows rolling averages with a 30-day window. The plot shows results for two FORHYCS runs, uncoupled (C_U) and fully coupled (C_F). For reference, the results obtained with standard PREVAH (C_P) are also shown. (b) Difference in simulated daily streamflow between the coupled and uncoupled versions of FORHYCS. Unlike in a), values are not shown as rolling averages. Streamflow simulated with coupled FORHYCS is usually higher than for the uncoupled version, and the greatest differences occur in winter and spring.

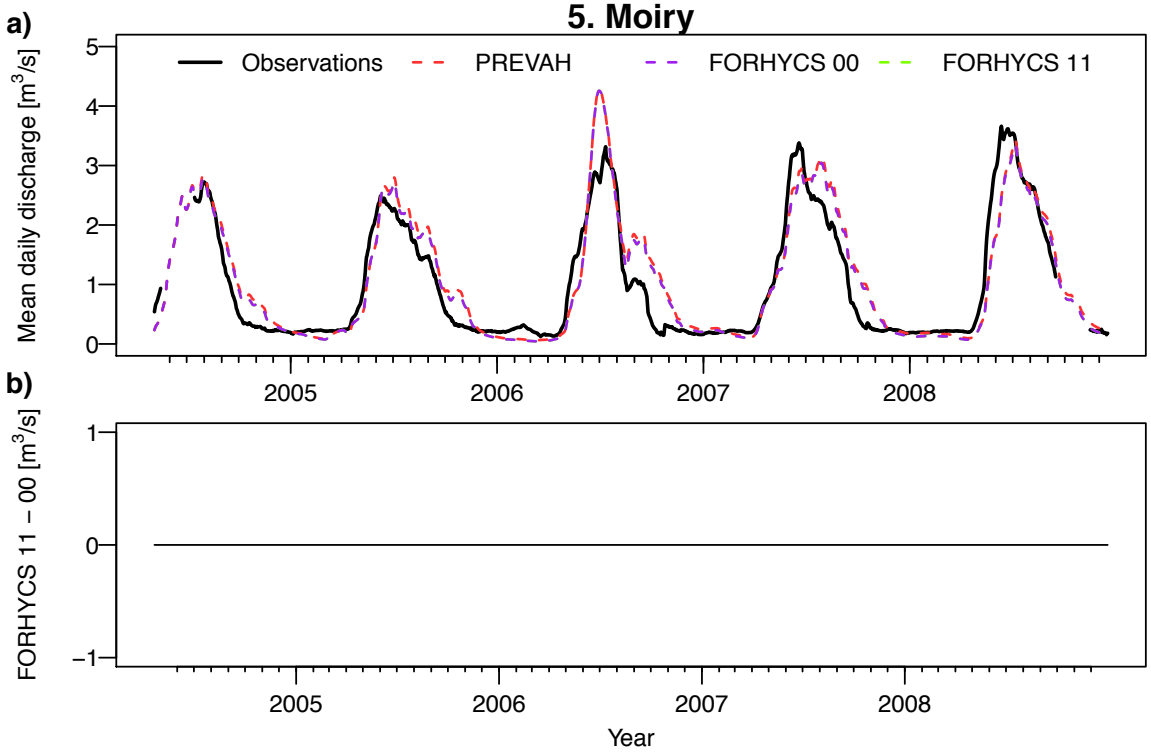

Figure S8: (a) Observed vs. simulated daily streamflow for subcatchment 5 (Moiry) for the period 2004-2008. For clarity, the plot shows rolling averages with a 30-day window. The plot shows results for two FORHYCS runs, uncoupled (C_U) and fully coupled (C_F). For reference, the results obtained with standard PREVAH (C_P) are also shown. (b) Difference in simulated daily streamflow between the coupled and uncoupled versions of FORHYCS. Unlike in a), values are not shown as rolling averages. Streamflow simulated with

coupled FORHYCS is usually higher than for the uncoupled version, and the greatest differences occur in winter and spring.

S2.2 Simulated biomass for other model configurations

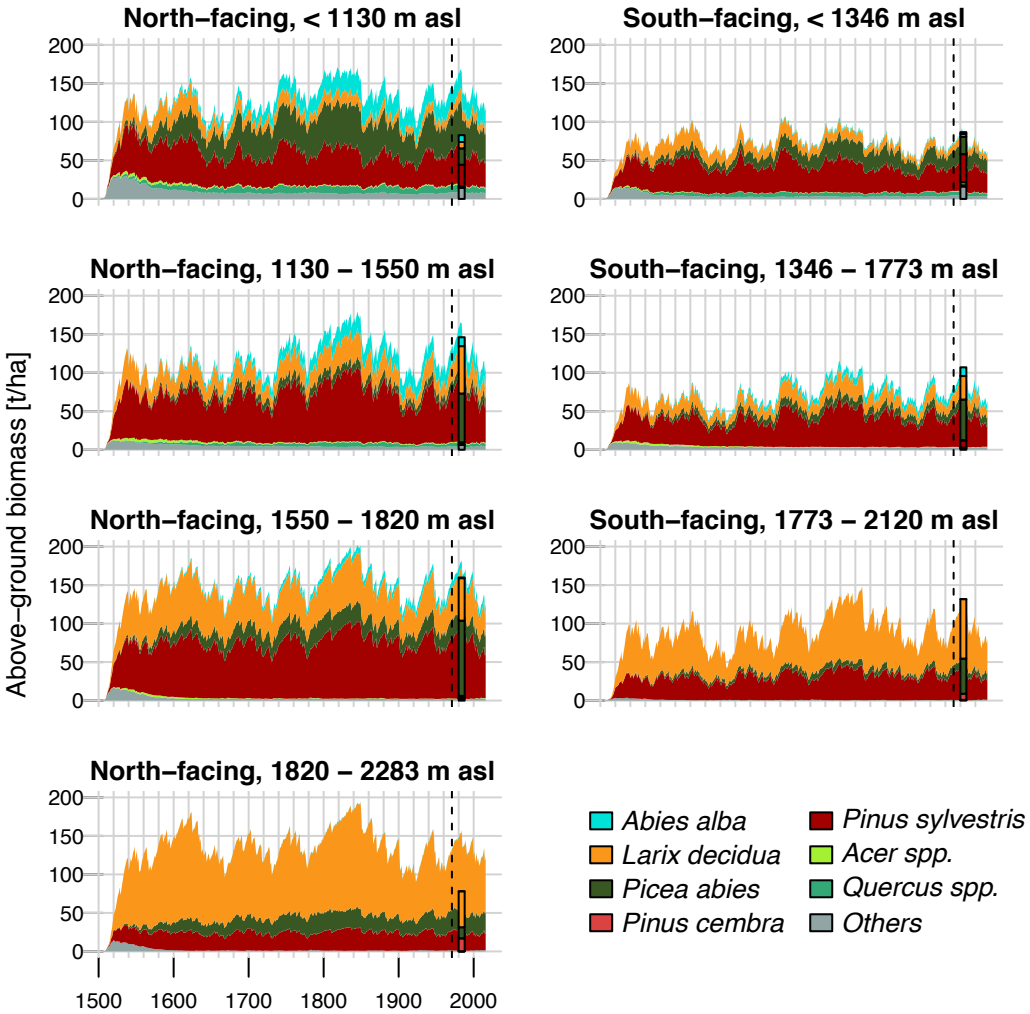

Figure S9: Aboveground tree biomass simulated with FORHYCS using the configuration S_T_noHmax_BEK (Table 1 – without height limitation). The graphs show annual values, averaged over seven clusters of cells. The bar shows the aboveground biomass in the same area, from the first Swiss national forest inventory (1982-1986; Bachofen et al., 1988). The limits of the elevation bands were set so that each cluster contains at least 30 forest inventory plots. The dashed line marks the year 1971, from when meteorological data are available. Simulation years before 1971 use meteorological data bootstrapped from the years 1981-2000.

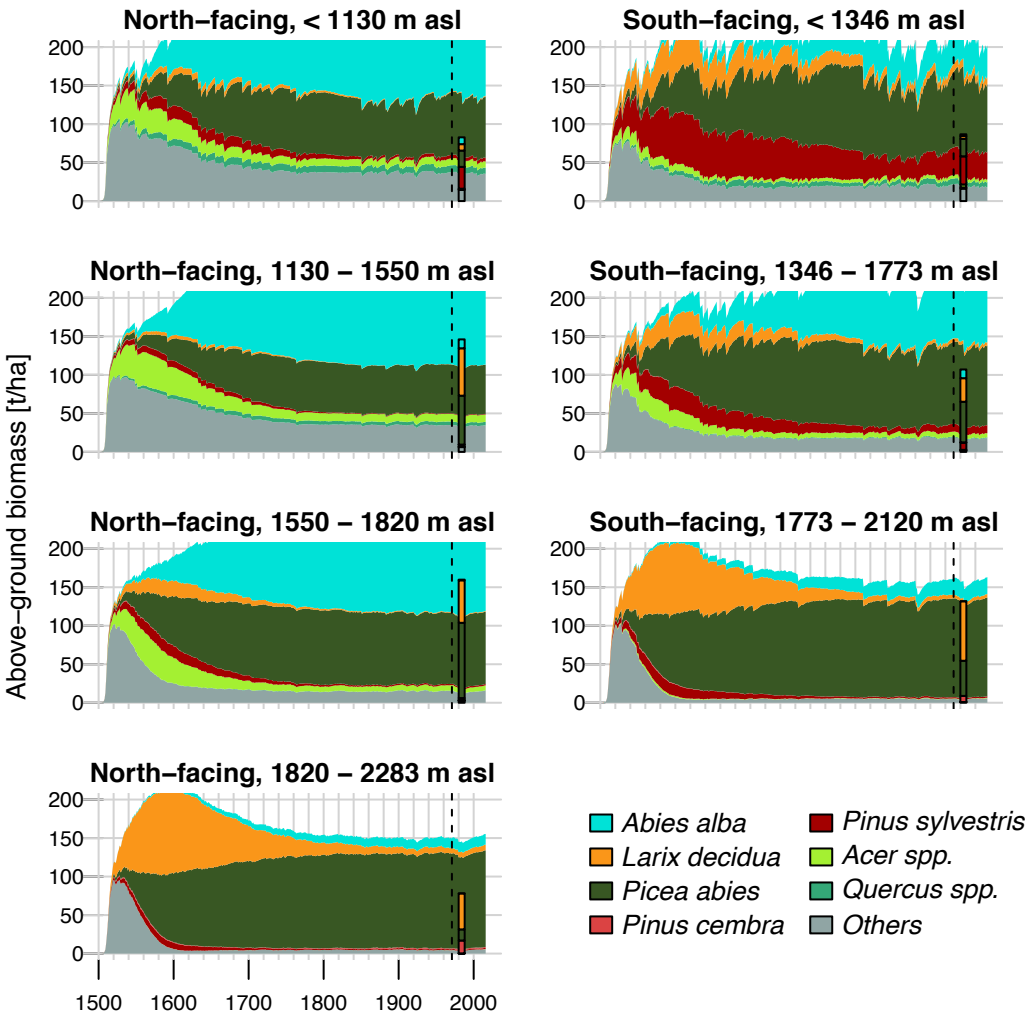

Figure S10: Aboveground tree biomass simulated with FORHYCS using the configuration S_T_noHmax_RA15 (Table 1 – without height limitation). The graphs show annual values, averaged over seven clusters of cells. The bar shows the aboveground biomass in the same area, from the first Swiss national forest inventory (1982-1986; Bachofen et al., 1988). The limits of the elevation bands were set so that each cluster contains at least 30 forest inventory plots. The dashed line marks the year 1971, from when meteorological data are available. Simulation years before 1971 use meteorological data bootstrapped from the years 1981-2000.

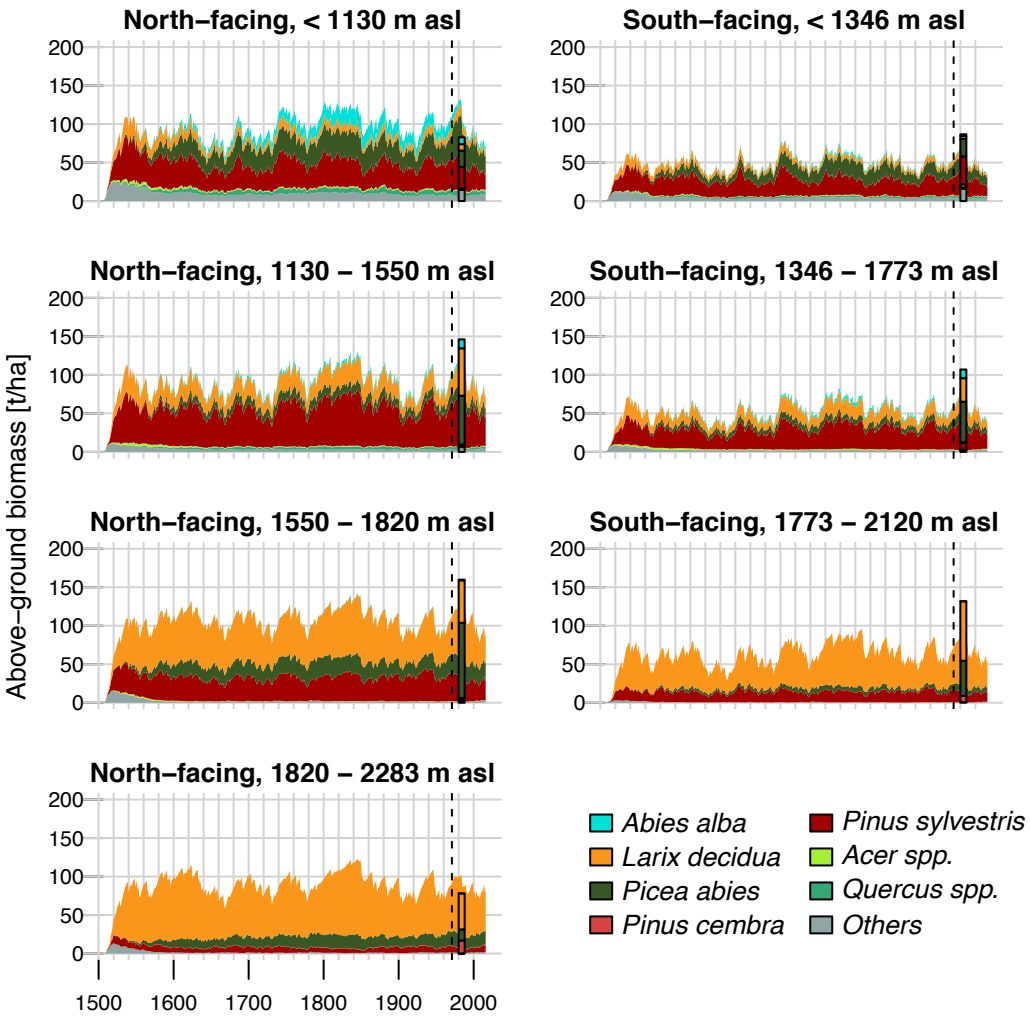

Figure S11: Aboveground tree biomass simulated with FORHYCS using the configuration S_T_Hmax_BEK (Table 1 – with height limitation). The graphs show annual values, averaged over seven clusters of cells. The bar shows the aboveground biomass in the same area, from the first Swiss national forest inventory (1982-1986; Bachofen et al., 1988). The limits of the elevation bands were set so that each cluster contains at least 30 forest inventory plots. The dashed line marks the year 1971, from when meteorological data are available. Simulation years before 1971 use meteorological data bootstrapped from the years 1981-2000.

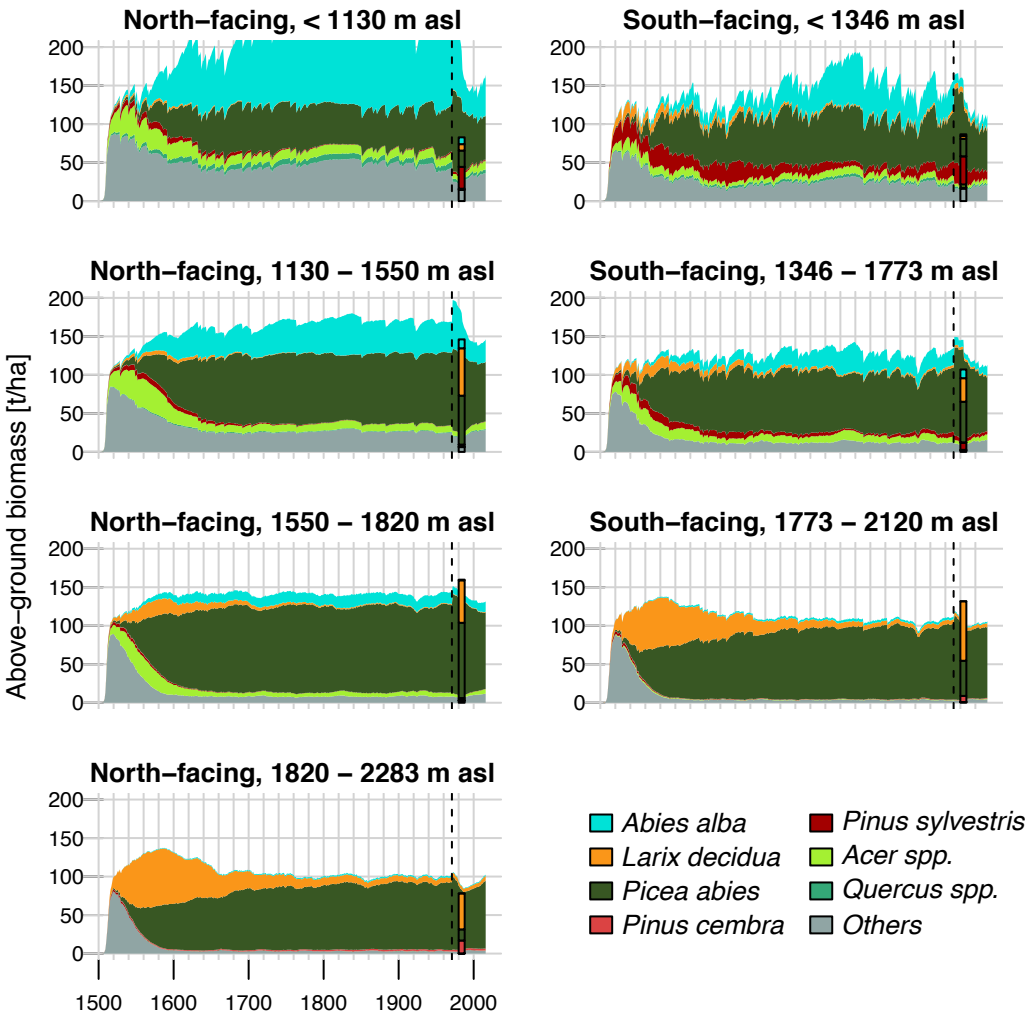

Figure S12: Aboveground tree biomass simulated with FORHYCS using the configuration S_T_Hmax_RA15 (Table 1 – with height limitation). The graphs show annual values, averaged over seven clusters of cells. The bar shows the aboveground biomass in the same area, from the first Swiss national forest inventory (1982-1986; Bachofen et al., 1988). The limits of the elevation bands were set so that each cluster contains at least 30 forest inventory plots. The dashed line marks the year 1971, from when meteorological data are available. Simulation years before 1971 use meteorological data bootstrapped from the years 1981-2000.

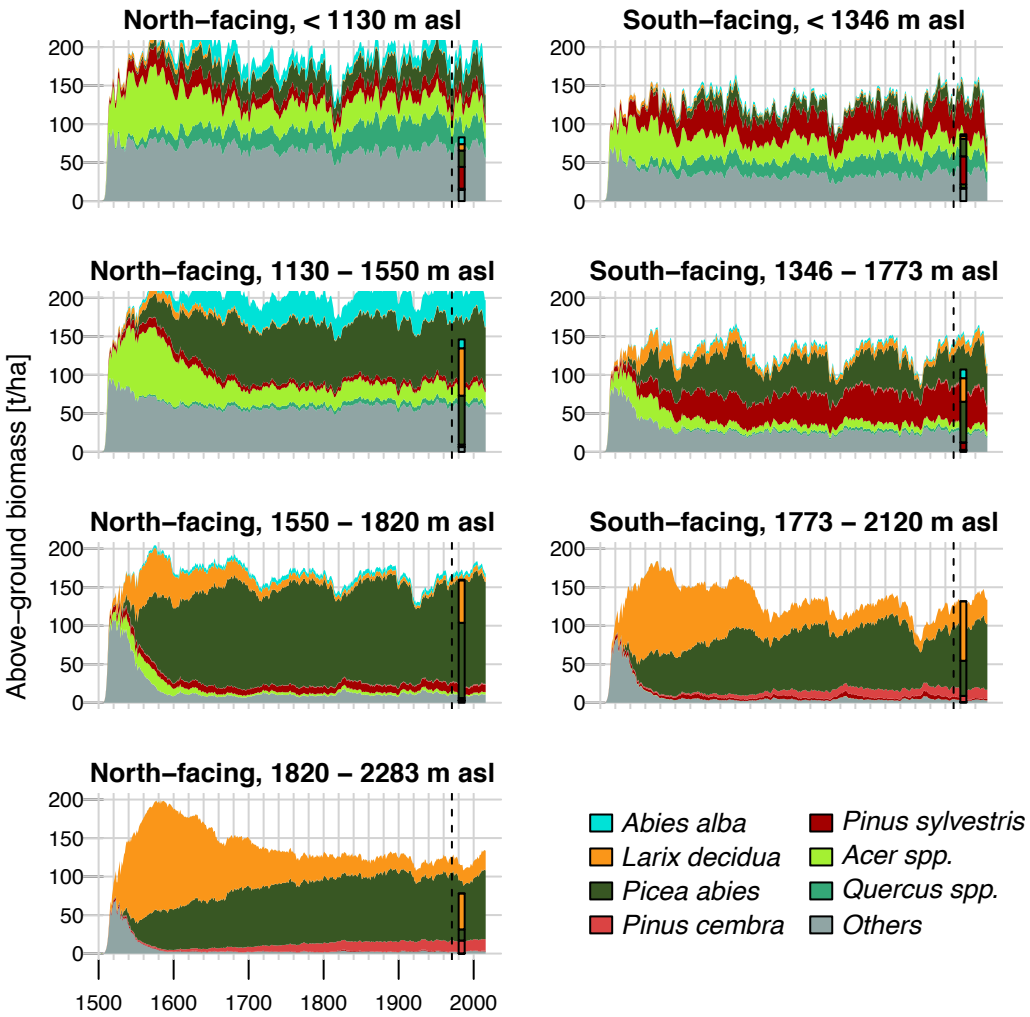

Figure S13: Aboveground tree biomass simulated with FORHYCS using the configuration S_F_Full (Table 1 – fully coupled run with all). The graphs show annual values, averaged over seven clusters of cells. The bar shows the aboveground biomass in the same area, from the first Swiss national forest inventory (1982-1986; Bachofen et al., 1988). The limits of the elevation bands were set so that each cluster contains at least 30 forest inventory plots. The dashed line marks the year 1971, from when meteorological data are available. Simulation years before 1971 use meteorological data bootstrapped from the years 1981-2000.

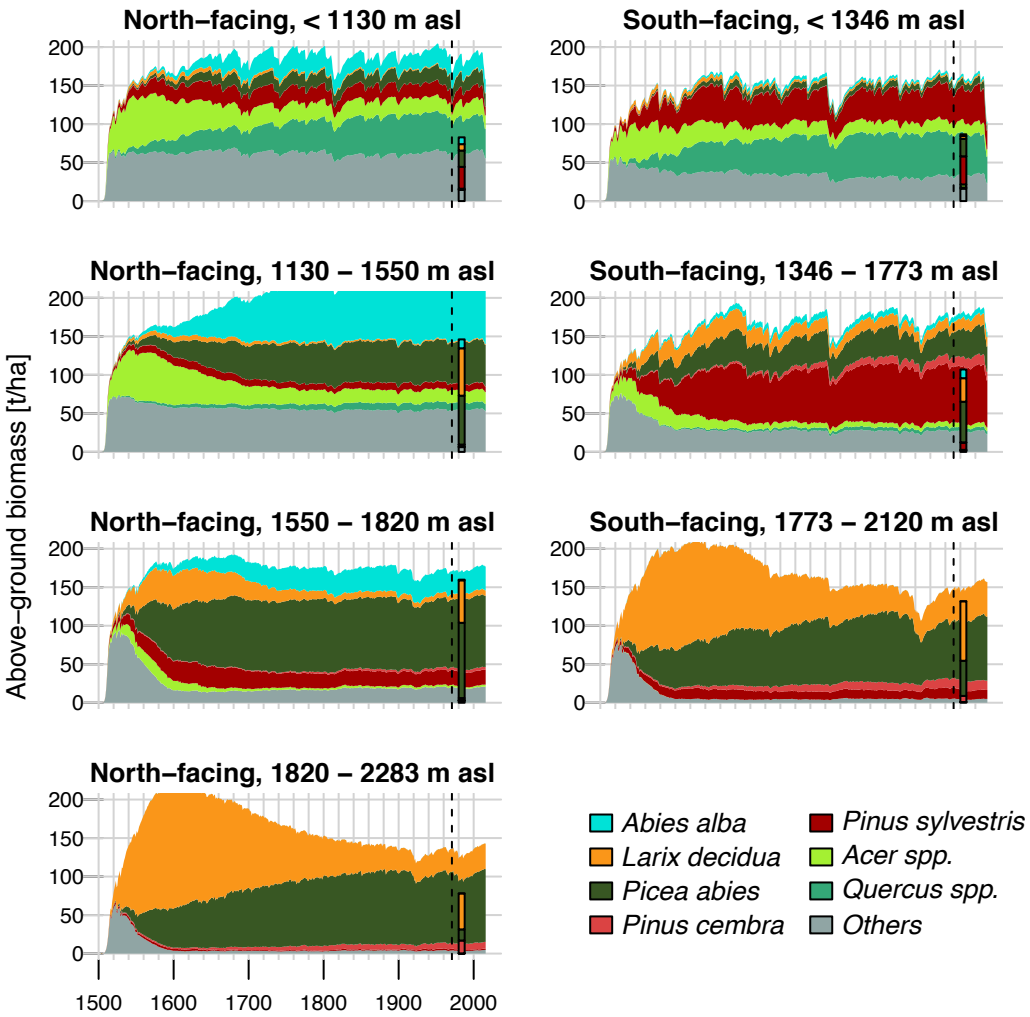

Figure S14: Aboveground tree biomass simulated with FORHYCS using the configuration S_F_noHmax (Table 1). The graphs show annual values, averaged over seven clusters of cells. The bar shows the aboveground biomass in the same area, from the first Swiss national forest inventory (1982-1986; Bachofen et al., 1988). The limits of the elevation bands were set so that each cluster contains at least 30 forest inventory plots. The dashed line marks the year 1971, from when meteorological data are available. Simulation years before 1971 use meteorological data bootstrapped from the years 1981-2000.

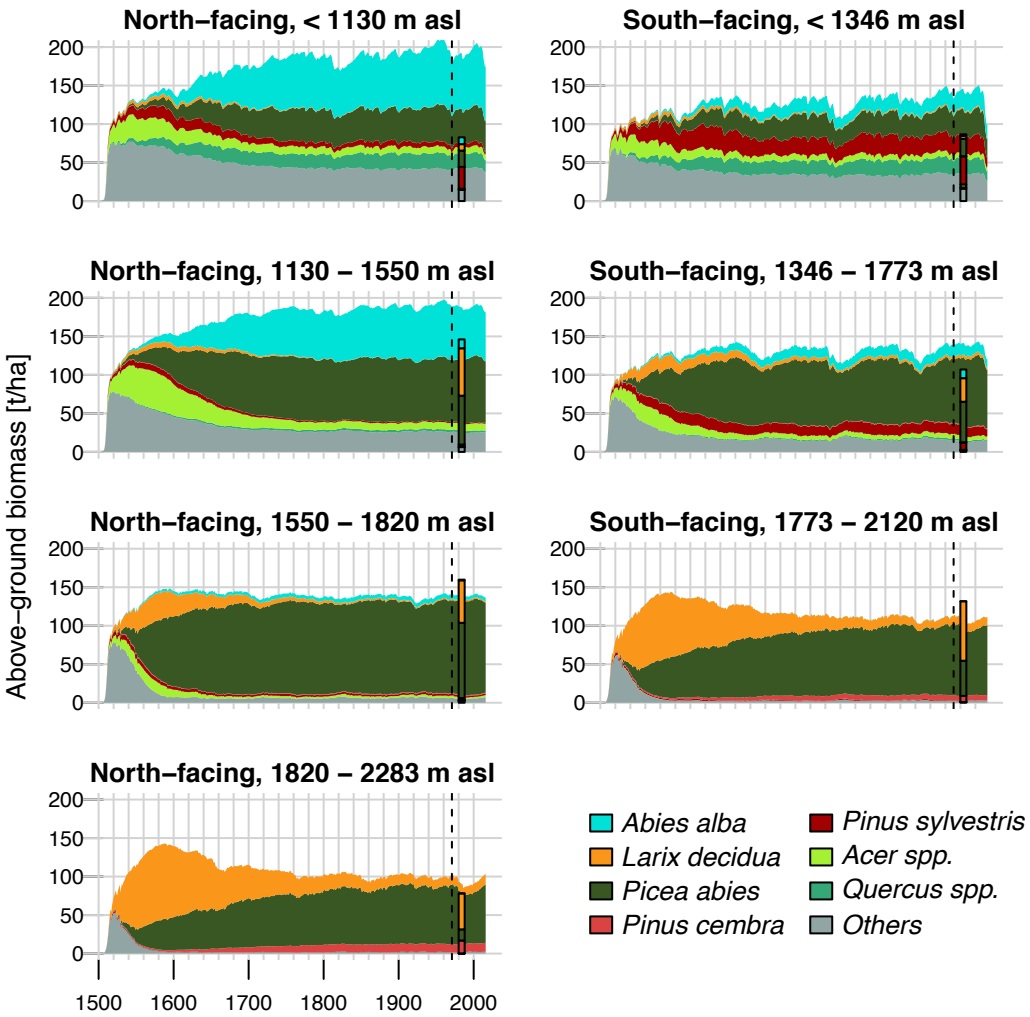

Figure S15: Aboveground tree biomass simulated with FORHYCS using the configuration S_F_cSFC (Table 1). The graphs show annual values, averaged over seven clusters of cells. The bar shows the aboveground biomass in the same area, from the first Swiss national forest inventory (1982-1986; Bachofen et al., 1988). The limits of the elevation bands were set so that each cluster contains at least 30 forest inventory plots. The dashed line marks the year 1971, from when meteorological data are available. Simulation years before 1971 use meteorological data bootstrapped from the years 1981-2000.

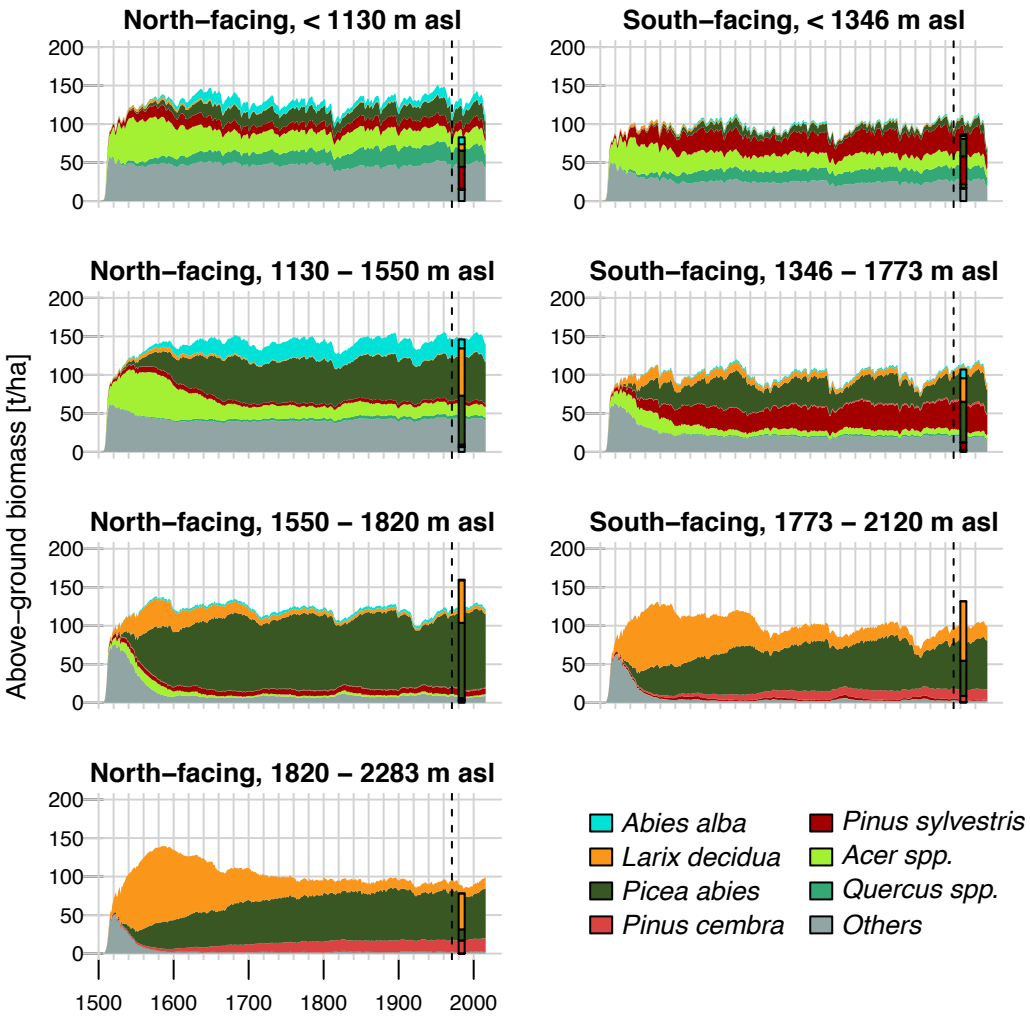

Figure S16: Aboveground tree biomass simulated with FORHYCS using the configuration S_F_noSmort (Table 1). The graphs show annual values, averaged over seven clusters of cells. The bar shows the aboveground biomass in the same area, from the first Swiss national forest inventory (1982-1986; Bachofen et al., 1988). The limits of the elevation bands were set so that each cluster contains at least 30 forest inventory plots. The dashed line marks the year 1971, from when meteorological data are available. Simulation years before 1971 use meteorological data bootstrapped from the years 1981-2000.

S2.3 Simulation results under climate change scenarios

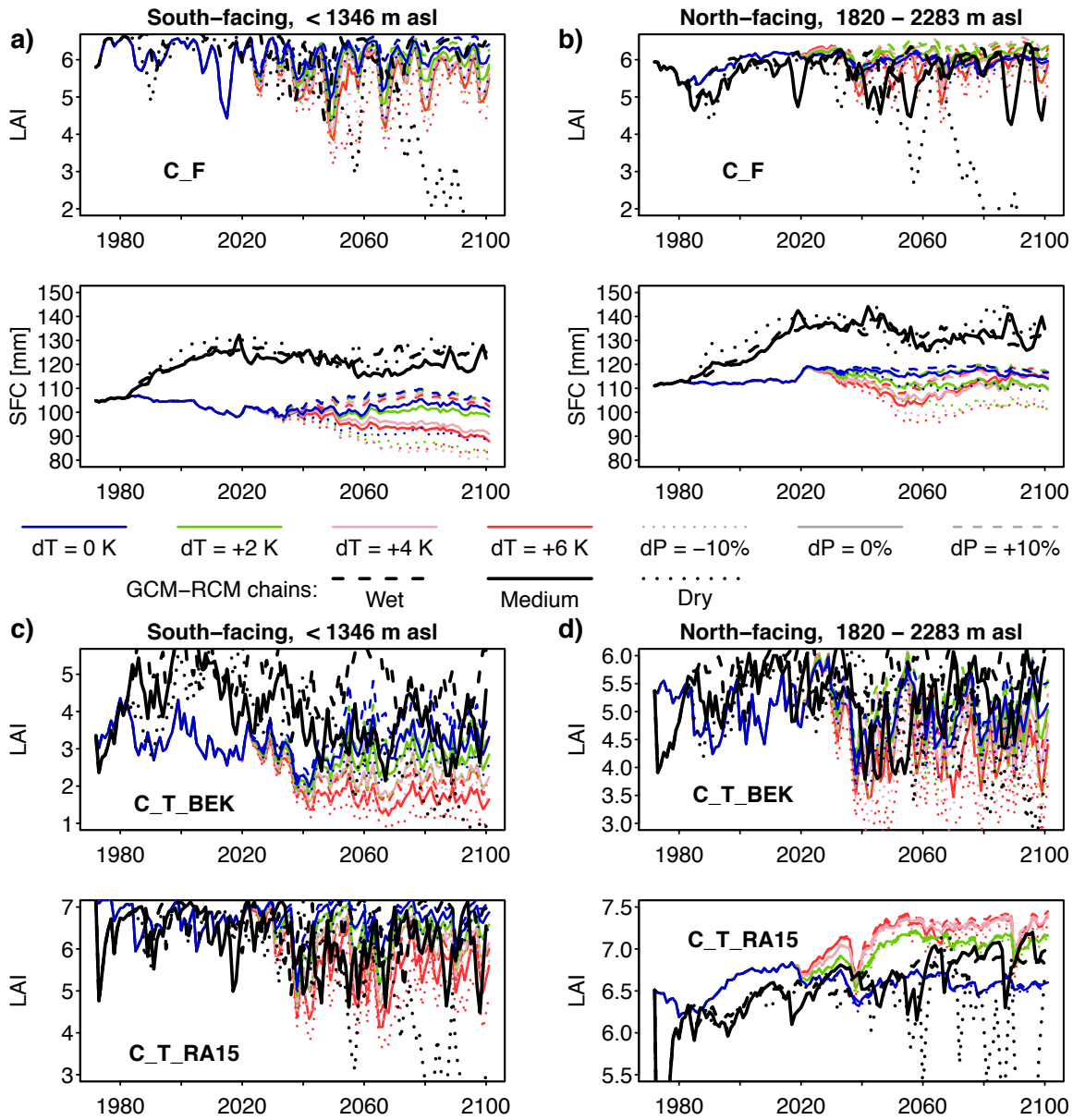

Figure S17: (a) Annual maximum LAI (top) and rooting zone storage SFC (bottom) under idealized climate change scenarios, simulated using coupled FORHYCS (C_F). LAI and SFC are averaged over the cells belonging to the lowest elevation class with south-facing slopes (same stratification as for Fig 6). LAI generally increases under wetting scenarios, and decreases under drying scenarios, although trends are not always monotonous. Similarly, SFC tends to increase with wetting and to decrease with drying. (b) Same as a), but for the highest elevation class with north-facing slopes. Also here, LAI increases under wet scenarios and decreases under dry scenarios. SFC trajectories show large differences between scenarios. (c) LAI simulated with TreeMig, with the two different soil parameterizations (C_T_BEK and C_T_RA15). Note the different scales on the y-axis. LAI simulated with C_T_BEK is markedly lower than for C_F, whereas the C_T_RA15 values are somewhat higher. (d) Same as c), but for the highest elevation class with north-facing slopes.

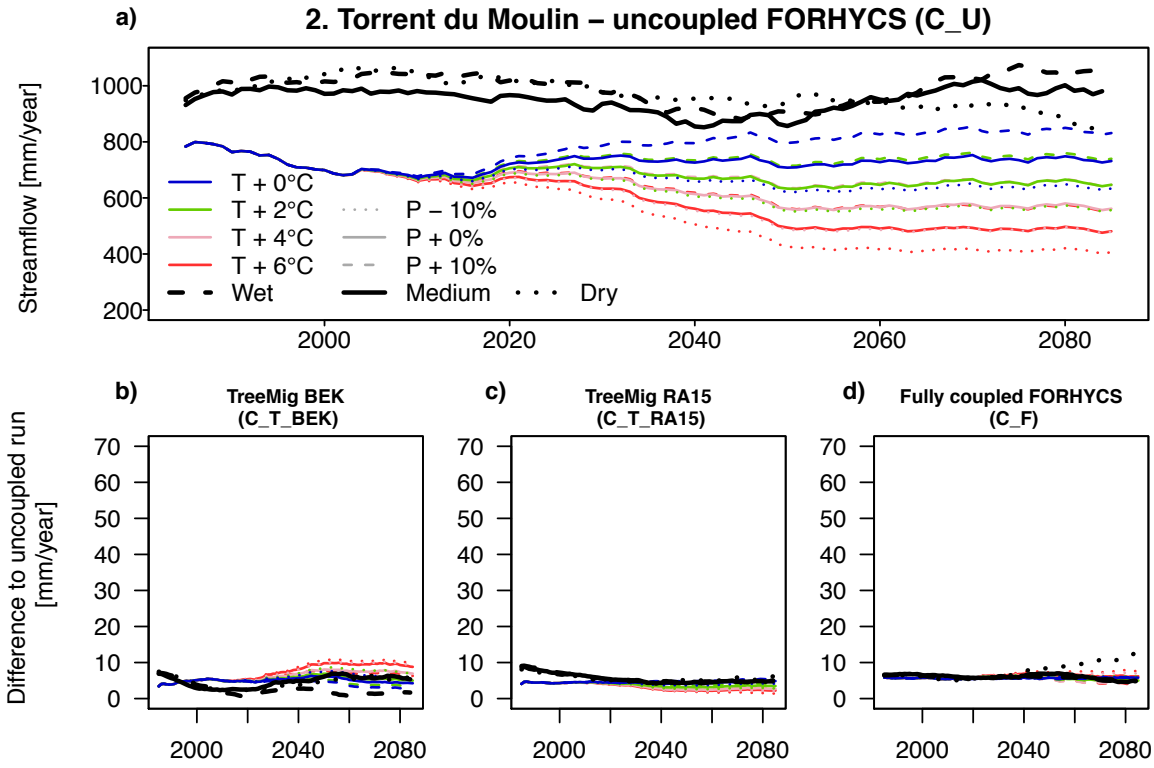

Figure S18: (a) Simulated annual streamflow (30-year rolling means) in the Torrent du Moulin subcatchment. In the warmest dry delta change scenario (T6_P-10), annual streamflow is reduced from 750 to less than 400 mm/year. (b) and (c) Difference in annual streamflow in the runs with one-way coupling, relative to the uncoupled run. (d) Difference in annual streamflow in the fully coupled FORHYCS run, relative to the uncoupled run. In all coupled runs, streamflow is greater than in the uncoupled version, due to lower LAI (see Fig. 8 and 9; the standard PREVAH value for forest LAI is 8) and, for the fully coupled version, smaller rooting zone storage capacity SFC.

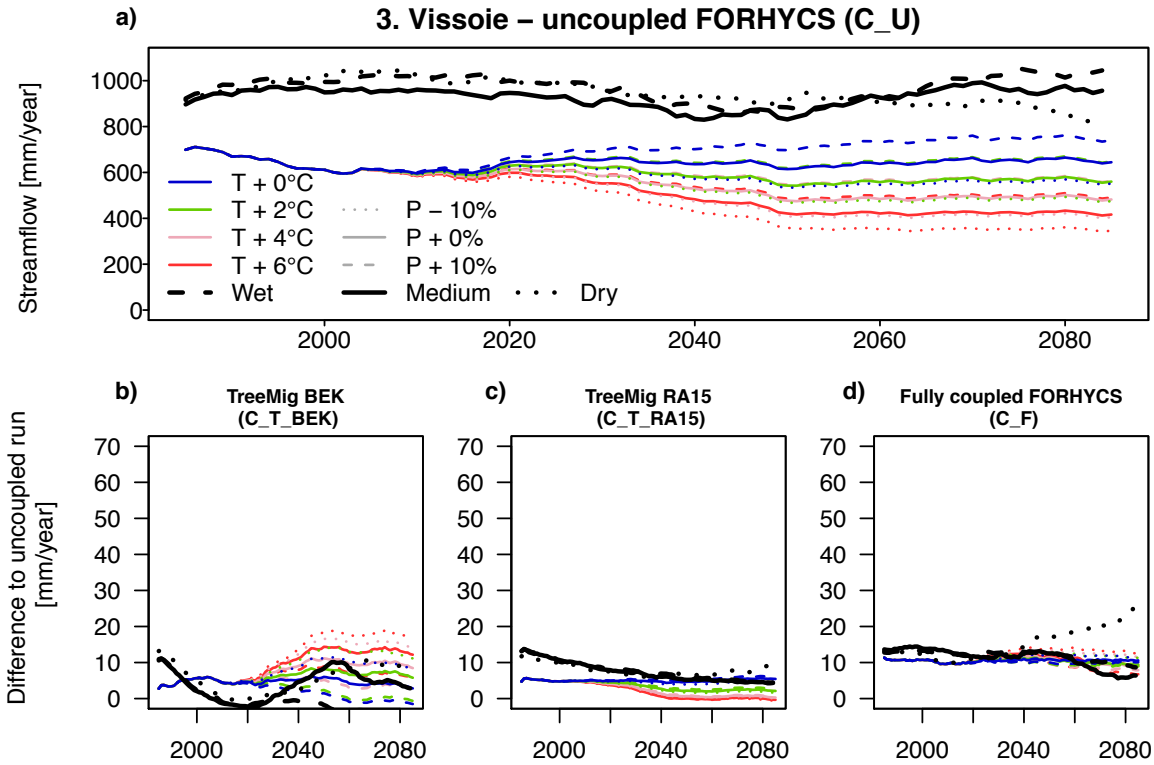

Figure S19: (a) Simulated annual streamflow (30-year rolling means) in the Vissoie subcatchment. In the warmest dry delta change scenario (T6_P-10), annual streamflow is reduced from 700 to less than 400 mm/year. (b) and (c) Difference in annual streamflow in the runs with one-way coupling, relative to the uncoupled run. (d) Difference in annual streamflow in the fully coupled FORHYCS run, relative to the uncoupled run. In all coupled runs, streamflow is greater than in the uncoupled version, due to lower LAI (see Fig. 8 and 9; the standard PREVAH value for forest LAI is 8) and, for the fully coupled version, smaller rooting zone storage capacity SFC.

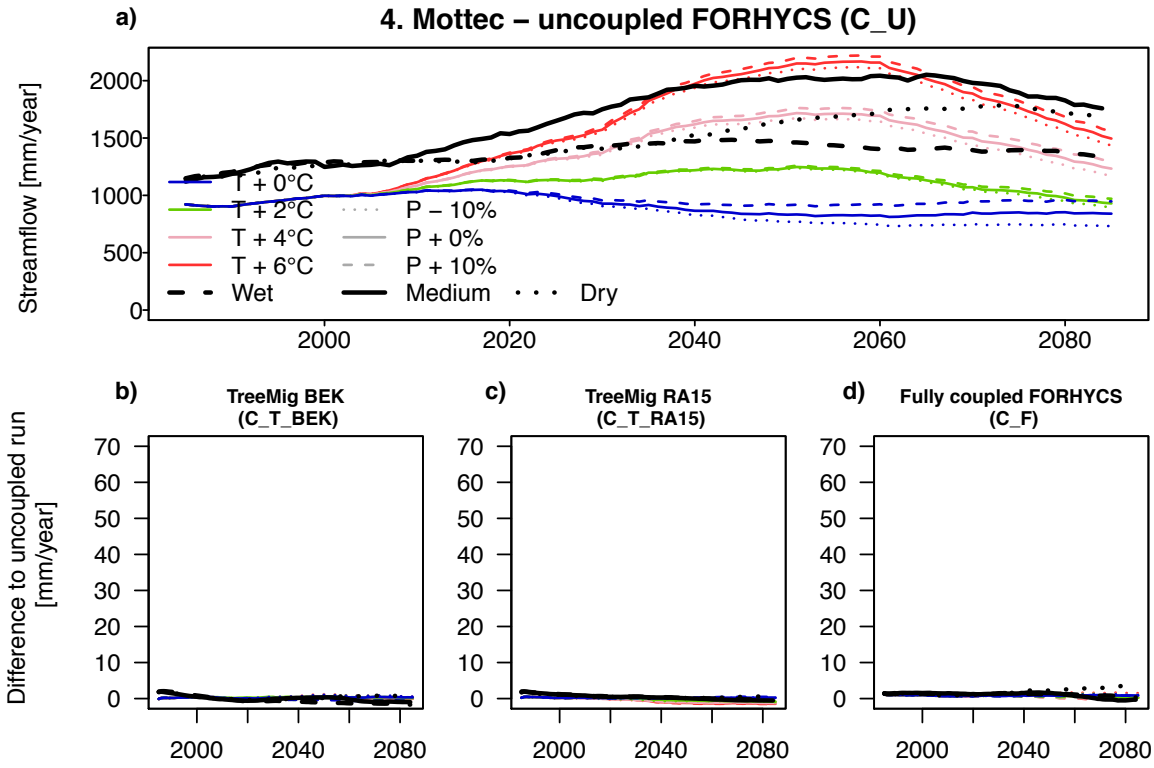

Figure S20: (a) Simulated annual streamflow (30-year rolling means) in the Mottec subcatchment. (b) and (c) Difference in annual streamflow in the runs with one-way coupling, relative to the uncoupled run. (d) Difference in annual streamflow in the fully coupled FORHYCS run, relative to the uncoupled run. In all coupled runs, streamflow is greater than in the uncoupled version, due to lower LAI (see Fig. 8 and 9; the standard PREVAH value for forest LAI is 8) and, for the fully coupled version, smaller rooting zone storage capacity SFC.

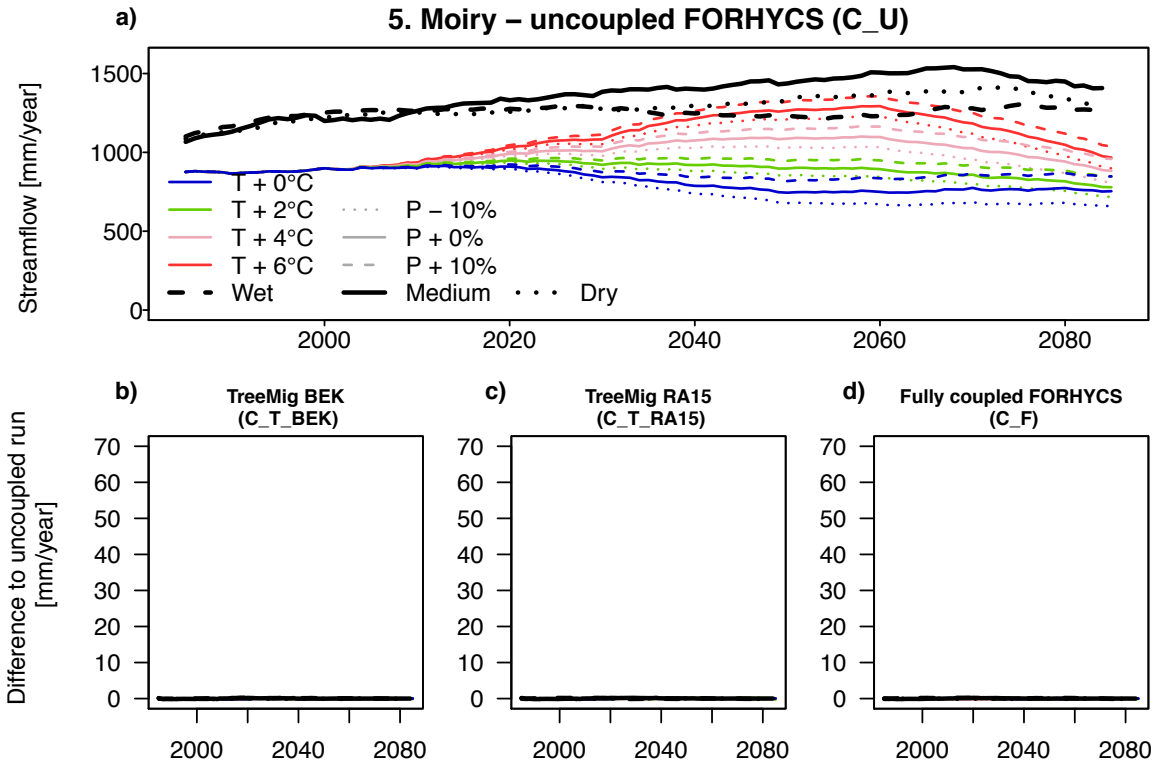

Figure S21: (a) Simulated annual streamflow (30-year rolling means) in the Moiry subcatchment. (b) and (c) Difference in annual streamflow in the runs with one-way coupling, relative to the uncoupled run. (d) Difference in annual streamflow in the fully coupled FORHYCS run, relative to the uncoupled run. In all coupled runs, streamflow is greater than in the uncoupled version, due to lower LAI (see Fig. 8 and 9; the standard PREVAH value for forest LAI is 8) and, for the fully coupled version, smaller rooting zone storage capacity SFC.

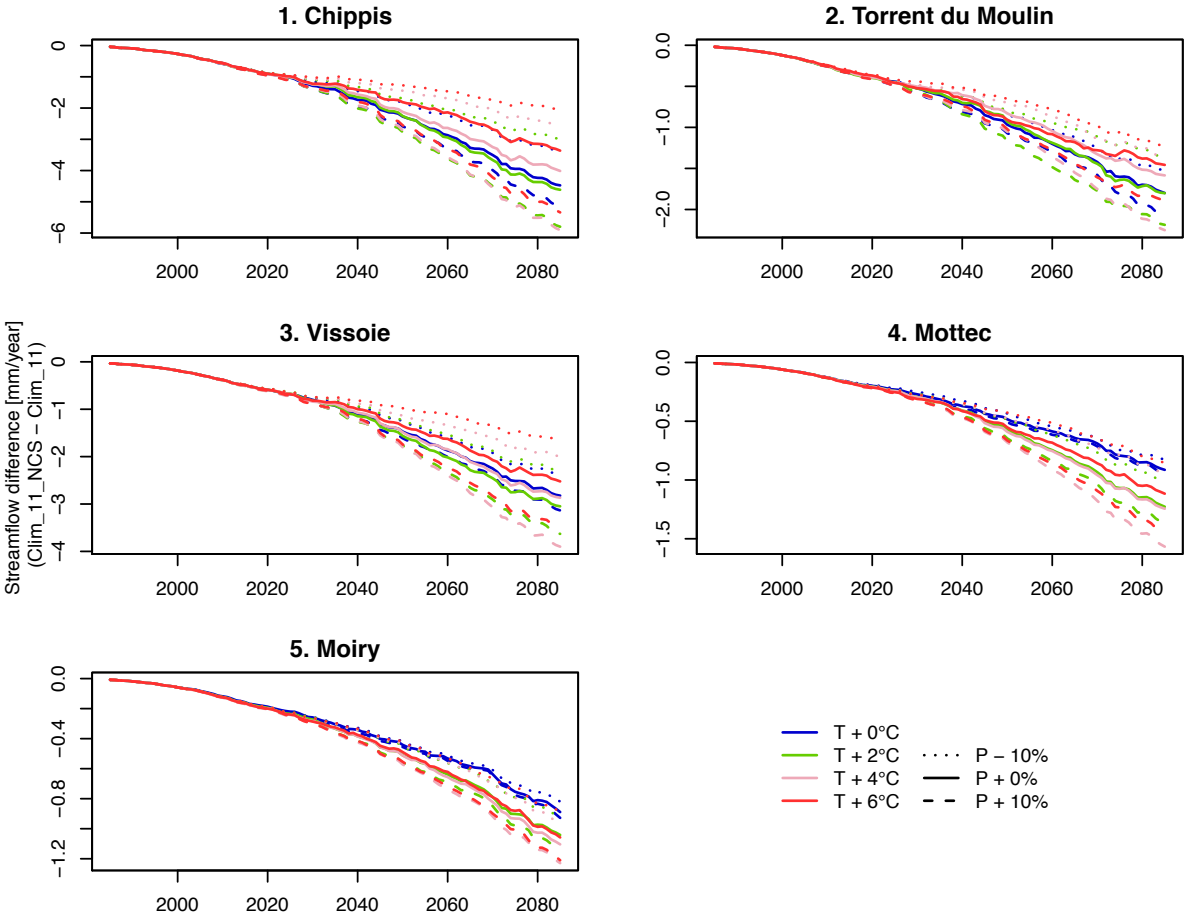

Figure S22: Differences in simulated annual streamflow between runs with CO2 effect on stomatal conductance switched off (C_F_NCS) and the standard runs with coupled FORHYCS (C_F), where this effect is switched on. The values are shown here as 30-year rolling means. Differences do not exceed 10 mm/year. In all cases, streamflow is lower under C_F_NCS.